AD NUMBER

AD475971

NEW LIMITATION CHANGE

TO

Approved for public release, distribution unlimited

FROM

Distribution authorized to U.S. Gov't. agencies and their contractors; Administrative/Operational Use; OCT 1965. Other requests shall be referred to Naval Ordnance Laboratory, White Oak, MD.

AUTHORITY

USNOL ltr, 29 Aug 1974

OCTOBER 1964 - OCTOBER 1965

FINAL TECHNICAL REPORT

NOL BALLISTICS RANGE PROGRAM ON ABRES RESEARCH

UNITED STATES NAVAL ORDNANCE LABORATORY
WHITE OAK, MARYLAND

U. S. NAVAL ORDNANCE LABORATORY
White Oak, Silver Spring, Maryland

FINAL TECHNICAL REPORT ON ABRES RESEARCH

NOL BALLISTICS RANGE PROGRAM

NOL Task NOL - 800/AF

20 October 1964 - 20 October 1965

U. S. NAVAL ORDNANCE LABORATORY
White Oak, Silver Spring, Maryland

FINAL TECHNICAL REPORT ON ABRES RESEARCH

NOL BALLISTICS RANGE PROGRAM

I. INTRODUCTION

The purpose of this program is to characterize the aerodynamic properties of the boundary layers and wakes of slender hypersonic vehicles by means of ballistics range data and their attendant analysis.

The Ballistics Range Program reported in this document is a portion of the ABRES program that is being provided by the U. S. Naval Ordnance Laboratory, White Oak, Maryland.

The NOL investigations have the following general objectives.

1. Measurement of aerodynamic properties that characterize the boundary layers and wakes of slender vehicles.
2. Evaluation of the experimental data to compare with existing theories.
3. Modification of current theory as required in the interpretation of the experiments.

II. PROGRAM

A. Task Identification

The major tasks, as identified in the Statement of Work, are as follows.

Task 1.0 Program Management

Task 2.0 Measurement of Turbulent Skin Friction on a Slender Cone

Task 3.0 Effect of High Heat Transfer Rates on Boundary Layer Transition

Task 4.0 Body Scale Effects on the Aerodynamic Characteristics of Wakes (Including Edge Roughness)

Task 5.0 The Effect of Heat Transfer on the Aerodynamic Characteristics of Wakes

Task 6.0 Data and Reports

The subjects under Task 1.0 are discussed in parts I, II, and III of this document.

Technical progress, problem areas, and methods of solution for major tasks 2.0 through 5.0 are each discussed in part IV under their respective task numbers.

B. Schedules

The schedules for major tasks and subtasks are presented in Table 1.1. The plan of approach and the degree of completion of subtasks are outlined in this table.

C. Program Organization and Direction

Work on ABRES research at the Naval Ordnance Laboratory was under the following administrative and technical direction.

Captain R. E. Odening, Commander, NOL
Captain J. A. Dare, Commander, NOL

Dr. G. K. Hartmann, Technical Director
Dr. R. E. Wilson, Associate Technical Director (Aeroballistics)
Dr. R. K. Lobb, Aeroballistics Program Chief
Dr. A. E. Seigel, Chief, Ballistics Department

All project work reported in this document was done in the Missile Dynamics Division (BR) of the Ballistics Department.

Work in the Missile Dynamics Division was under the direction of Mr. W. C. Lyons, Jr., Chief, Missile Dynamics Division from October 1964 to August 1965 and under the direction of Mr. J. L. Lankford, Acting Chief, Missile Dynamics Division from September 1965 to completion of this contract.

Project Personnel

Many individuals have contributed directly and indirectly to the work of this program. The following list contains only those responsible for major task assignments.

Task 1.0 - Coordination, preparation, compilation and editing of monthly letter reports, quarterly technical reports, and final technical reports - Mr. John L. Lankford

Task 2.0 - Turbulent Skin Friction on Slender Cones - Mr. W. Carson Lyons, Jr., and Mr. John L. Lankford

Task 3.0 - Effect of Heat Transfer on Boundary Layer Transition - Mr. Norman W. Sheetz, Jr.

Task 4.0 - Body Scale Effects on Wake Characteristics - Mr. Zigurds J. Levensteins and Mr. Maigonis V. Krumins

Task 5.0 - Effect of Heat Transfer on Wake Characteristics - Mr. Zigurds J. Levensteins and Mr. Maigonis V. Krumins

Model and Sabot Design and Launching Techniques - Mr. L. E. Crogan, Mr. S. L. Hanlein, and Mr. R. G. Schuetzler

Data Reduction - Miss A. A. Chamberlin

Machine Programming - Mr. H. S. Brown

D. Reports

All experimental work and major results of analytical and computational work, as indicated in the schedule of Table 1.1, are reported in this document to fulfill requirements of the Statement of Work for the period of October 1964 to October 1965. This report comprises the final technical report as required by the Statement of Work. Subsequent to this report, separate NOL Technical Reports will be prepared on each of the major subject areas covered in this program. These documents which represent official NOL publications will be written and distributed in accordance with the general Navy requirements for such official reports and will contain all evaluation, analyses, and data available in their respective subject areas at the time of their completion. These publications are scheduled for completion and distribution within the next six to twelve months.

III. EXPERIMENTAL FACILITIES

All experimental tasks in the NOL Ballistics Range Program were carried out in either the NOL 1000-foot Hyperballistics Range (figure 1.1 and Table 1.2) or in the NOL Pressurized Ballistics Range (figure 1.2 and Table 1.3).

The general characteristics of these facilities are listed in the reference tables and figures. Specific capabilities of importance to individual tasks are discussed under appropriate task headings in part IV of this report.

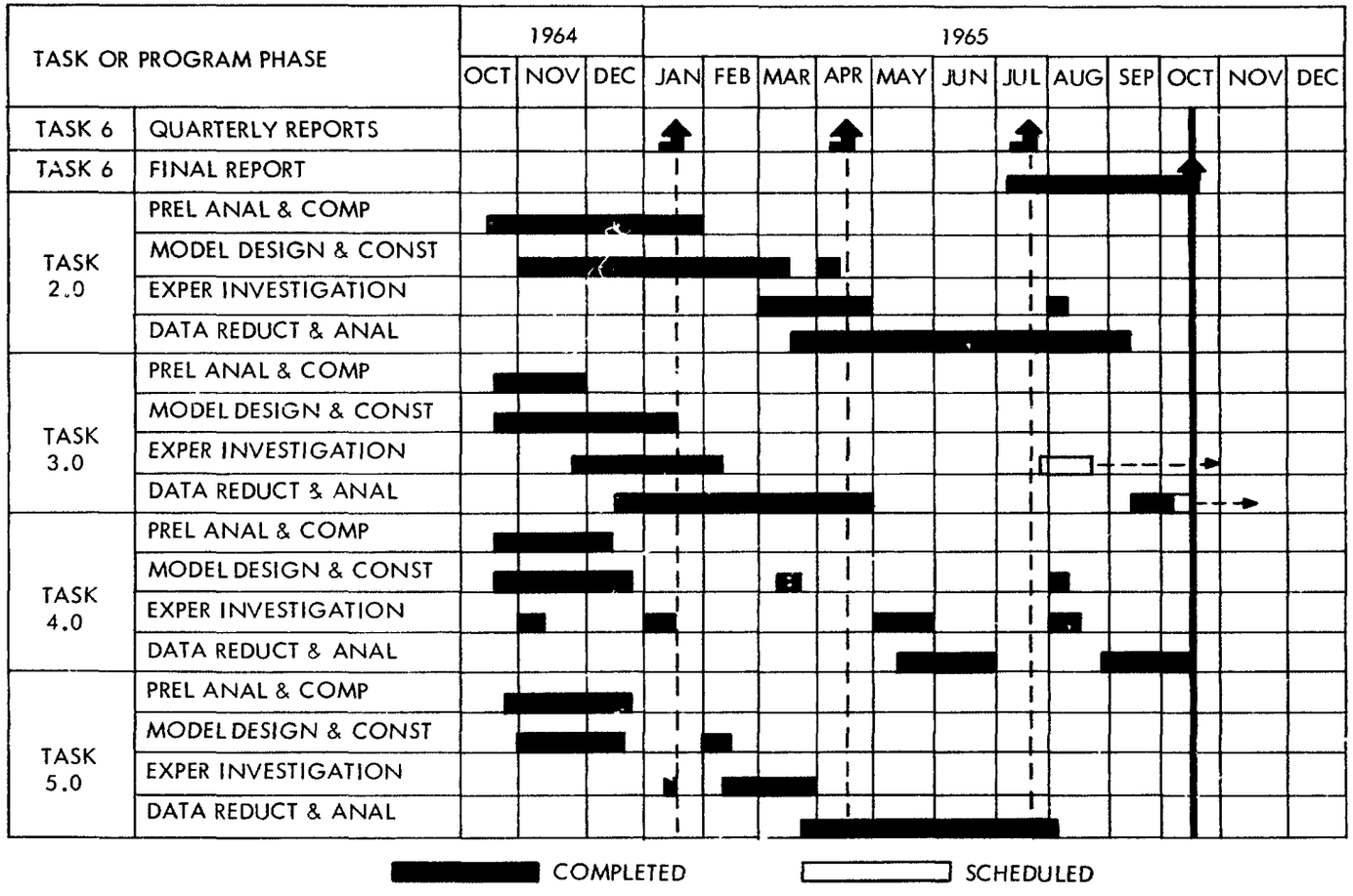

TABLE 1.1 PROGRAM AND SCHEDULES - NOL ABRES BALLISTICS RANGE PROGRAM

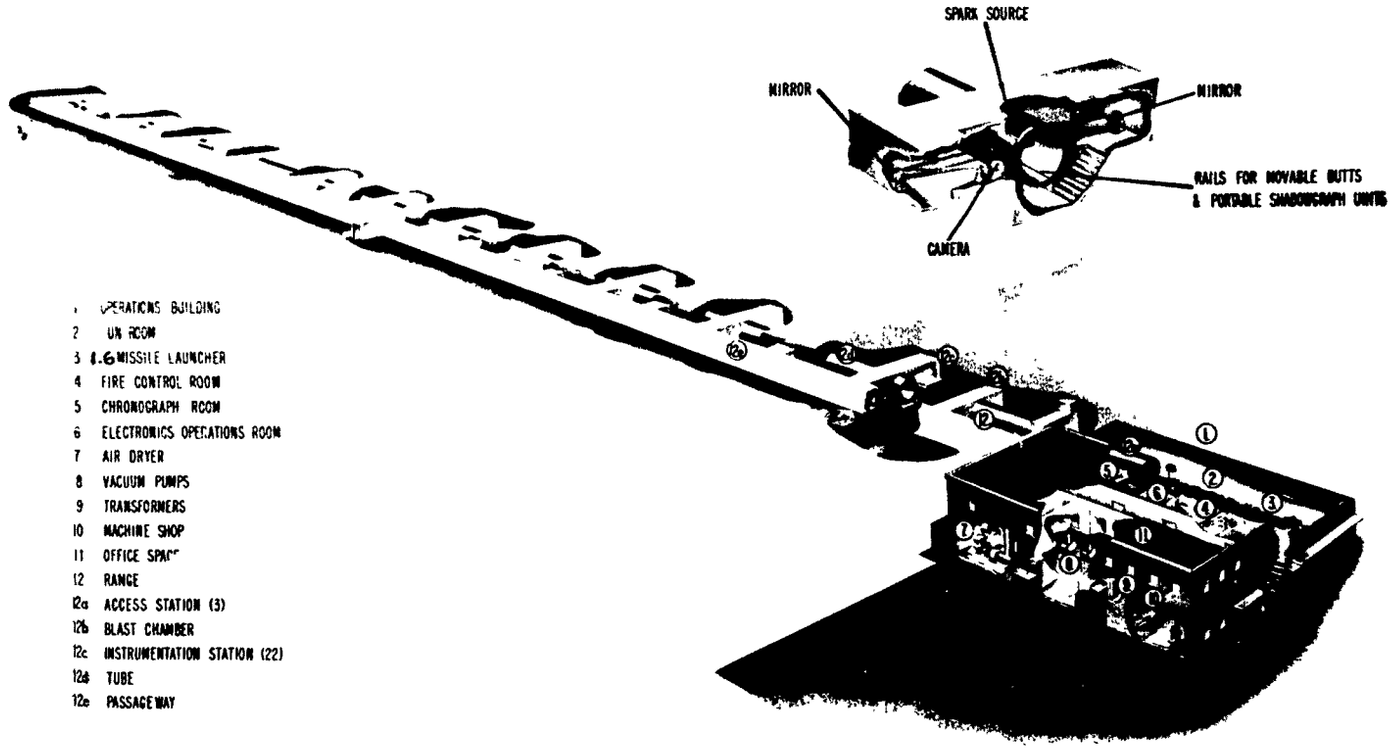

FIG. 1.1 N.O.L. 1000FT. HYPERBALLISTICS RANGE

TABLE 1.2 CHARACTERISTICS OF THE NOL 1000-FOOT HYPERBALLISTICS RANGE*

1000-FOOT HYPERBALLISTICS RANGE

This range has the following characteristics

Length:	1,000 ft. Usable testing length for drag - 785 ft. Usable testing length for stability - 340 ft.
Cross Section:	10-ft. diameter with usable dispersion area of 2 x 2 ft.
Pressure:	1 atmosphere down to 3×10^{-4} atmosphere
Temperature:	65°F ambient
Maximum Projectile Size:	2 in. diameter (varies with barrel size)
Velocity Range:	5,000 - 21,000 ft/sec
Launchers:	Two-stage light-gas guns 1.6" x 384 cal. 2.48" x 200 cal.
Photographic Spark Stations:	27 reflector shadowgraph stations, 1 experimental laser station, 3 schlieren stations
Additional Capabilities:	C and K band focused microwave interferometers, 3 spectrophotometers for radiation studies 12 luminosity stations

*This table reflects changes made during the course of this program.

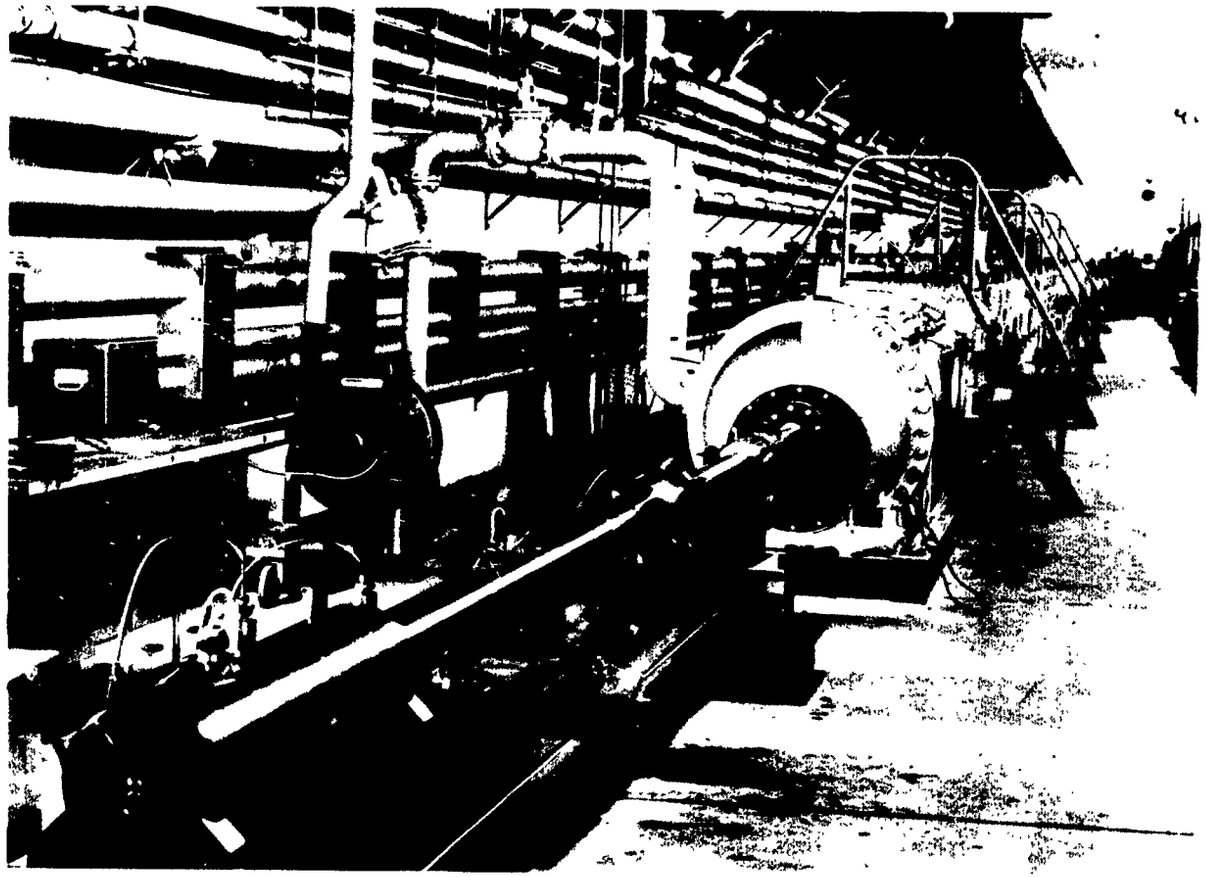

FIG. 1.2 N.O.L. PRESSURIZED BALLISTICS RANGE

TABLE 1.3 CHARACTERISTICS OF THE NOL PRESSURIZED BALLISTICS RANGE*

PRESSURIZED BALLISTICS RANGE

This range has the following characteristics:

Length:	285-ft. tube 189 ft. usable length for drag and stability measurements
Cross Section:	3-ft. diameter where 14 x 17 in. shadowgraphs of model and wake are made
Pressure:	6 atmospheres absolute to 4/1000 of an atmosphere (123,000 ft. altitude)
Temperature:	75°F ambient
Maximum Projectile Size:	2 in. in a powder gun 1 in. in the two-stage gas gun
Velocity Range:	1,000 - 24,000 ft/sec dependent upon gun, projectile size and charge
Launchers:	Two-stage light-gas guns: .822" x 375 cal.; .788" x 240 cal.; 1.261" x 230 cal.; 1.000" x 400 cal. Powder guns: 76-40 mm x 144" long; 57 mm x 72" long; 40 mm x 60" long
Photographic Spark Stations:	27 shadowgraph stations, 2 high sensitivity double-pass schlieren stations
X-Ray Stations:	2
Additional Capabilities:	Controlled temperature section (80 - 800°F); gas chromatograph; 3 spectrophotometers for radiation studies Specially instrumented 21-ft. section for continuous coverage wake photographs

*This table reflects changes made during the course of this program.

IV. RESULTS OF NOL BALLISTICS RANGE PROGRAMS (Oct 1964 - Oct 1965)

General

The general objectives of all major tasks have been met and substantial new experimental results of interest have been obtained. The complete range of test parameters originally desired has been limited in some instances by difficulties encountered in the state of the art in launching hypervelocity models over a wide range of conditions.

Information on statistical wake studies, extension of information on transition Reynolds number, and results on model base effects beyond the requirements of the original Statement of Work have been included under the appropriate task report.

Summary of Results

Measurement of total drag as an index of turbulent hypersonic skin friction has been demonstrated as a feasible experimental technique.

The contribution of skin friction drag coefficient for a 6.3-degree half-angle cone of .03 nose to base radius ratio varies from approximately 22 percent of the total at Mach number 6 to approximately 38 percent of the total at Mach number 15. The accuracy with which the experimental drag can be measured and the theoretical components estimated permit comparison of several theories through the Mach number range of 6.25 to 14 for low values of wall to recovery temperature ratio. (Task 2.0)

Launchings with a closed and an open model base showed no measurable difference in drag.

New information on transition at Mach numbers between 6 and 14 has permitted a better definition of the variation of transition Reynolds number with Mach number. (Task 2.0)

Previous work on the effect of heat transfer on transition has been extended to higher Mach numbers and lower temperature ratios (wall to recovery). In general, a destabilizing effect on the boundary layer was produced by decreasing the ratio of the wall temperature to the recovery temperature. Experimental data have been obtained at Mach number 8 and ambient range temperatures of 80°F, 200°F, and 400°F. (Task 3.0)

A temperature controlled section of the NOL Pressurized Ballistics Range has been utilized to obtain realistic simulation of wall to stagnation enthalpy ratios for hypersonic flight. Employing this experimental technique, the effects of enthalpy ratio upon wake characteristics have been investigated on a 9-degree half-angle cone with a 0.05 nose to base radius ratio. (Tasks 4.0 and 5.0)

In general, results indicate that the Reynolds numbers of transition based upon free-stream conditions and the distance from the model base to transition in the wake decrease with decreasing values of wall to stagnation enthalpy ratio. (Task 5.0)

For the conditions investigated, the enthalpy ratio appeared to have little or no effect upon the distance between recompression shocks. The effect on the distance to the recompression shock was inconclusive due to limited data and the difficulty of seeing more detail in heated range shadowgraphs. (Task 5.0)

An investigation was made of body scale effects and Reynolds number effects on the laminar to turbulent wake transition characteristics for a 9-degree half-angle cone.

Above a certain maximum value of body Reynolds number for a given Mach number, the transition from laminar to turbulent flow will occur on the body or in the base flow. In an intermediate range of body Reynolds numbers the wake transition Reynolds number appears to be constant and independent of body Reynolds numbers for fixed values of Mach number. (Task 4.0A)

Little quantitative information was obtained at low body Reynolds numbers, but it is apparent that the wake transition Reynolds numbers are greater and not constant as was the case at intermediate values. (Task 4.0A)

The turbulent wake edge behavior was described in terms of statistical parameters. It was found that the intermittency distribution is Gaussian and remains so with distance downstream. It was also found that the standard deviation and correlation microscale increase with distance downstream. (Task 4.0B)

RECOMMENDATIONS FOR FUTURE WORK

General

There is a need for additional work on transition and the effects of heat transfer on transition by means of an experimental program so designed that the relation of Mach number effect, unit Reynolds number and bluntness can be more clearly defined and understood.

Investigations of the wake characteristics through a wide range of enthalpy ratios are required to provide a better understanding and definition of the effects of this parameter.

Experimental Techniques

Hyperballistics ranges are providing urgently needed experimental results on the characteristics of slender vehicles at hypersonic velocities. In order to continue to advance in this work it is necessary to constantly experiment with new ideas and techniques to provide more extensive and accurate experimental data.

During the course of this program, several areas requiring intensive development have become apparent:

(1) Improved techniques for launching small models at low pressures with low angle of yaw are needed.

(2) Techniques for model design and launching are needed to provide the capability of launching relatively large slender models at high velocities and pressures without excessive nose recession or distortion. (New materials and fabrication methods)

(3) Improved techniques are needed for designing, launching, and observing ablation models.

(4) Improved techniques using temperature controlled sections are required to provide information on slender bodies through a wider range of heat transfer conditions.

(5) Excessive luminosity in some cases has caused severe problems with optical observations. Improved techniques are needed for obtaining high quality optical data on luminous models.

TASK 2.0

MEASUREMENT OF TURBULENT SKIN FRICTION ON A SLENDER CONE

Introduction

The drag of slender bodies traveling at hypersonic velocities can contain a component due to skin friction that is of the order of 35 percent of the total.

In the case of a vehicle with transition on the body, the skin friction will be made up of both laminar and turbulent components. For the case where transition is close to the nose of the body, the laminar component will usually be small since it affects a relatively small area. In such cases, the evaluation of the hypersonic turbulent skin friction drag is a major problem in the determination of total drag.

Theory and analysis have been of limited value in evaluating specific cases of turbulent skin friction at high Mach numbers. This condition exists because although general agreement is found among theories on some points such as the effects of heat transfer, current theories show poor quantitative agreement in many cases. A situation of this nature places extreme importance upon available experimental results; but, unfortunately, measurements of hypersonic skin friction are very scarce. This is due primarily to the difficulty encountered in obtaining a turbulent boundary layer on models tested in ground-based facilities. A survey of available literature indicates that most data have been obtained at Mach numbers below 6.

Symbols

C_{D_o} = Total drag coefficient

C_{D_B} = Drag coefficient due to base drag

C_{D_p} = Drag coefficient due to pressure drag

C_{D_F} = Drag coefficient due to turbulent skin friction

(Drag coefficients based upon base area)

L = Axial length of model

M_∞ = Free-stream Mach number based upon mid-range velocity and range conditions

P = Local static pressure

P_∞ = Free-stream static pressure

q_∞ = Free-stream dynamic pressure

R_{∞_L} = Reynolds number based upon free-stream conditions and axial length

$R_{\infty_{tr}}$ = Reynolds number of transition based upon free-stream conditions

S = Wetted length of model

α = Angle of attack

θ_c = Half angle of cone

Description of Models and Tests

In the NOL 1000-foot Hyperballistics Range (figure 1.1 and Table 1.2) there exists the capability of launching slender cones approximately five inches long at a velocity of 15,000 feet per second and cones approximately four inches long at about 18,000 feet per second. Range pressure can be regulated so that turbulent flow will exist over most of the cone surface. Model position can be determined to within 0.02 foot in the 880 feet of instrumented length and arrival time determined to within 0.2 microsecond. This permits experimental determination of total drag coefficient with an accuracy of approximately 2 percent. Since hypersonic turbulent skin friction drag is a significant part of total drag at these conditions, it is possible to evaluate the skin friction component from such measurements of total drag. Present tests were conducted at Mach numbers from 6.25 to 14.

In order to obtain hypersonic model velocities without excessive initial accelerations, it is important in ballistics range experiments to keep the "in-gun" weight of model and sabot as low as possible. It is also important to locate the center of gravity of the model in such a position that successful launches and stable flights will result. At pressures that will give turbulent flow on range models, it is also necessary to select materials that will keep ablation and luminosity within acceptable limits. It is often difficult to meet all of these, sometimes, conflicting requirements.

The greater part of the data for this task was obtained with models of the type shown in figures 2.1 and 2.2. Models were 6.3-degree half-angle cones with nose to base radius ratio of 0.03. Data for lower Mach numbers were obtained with homogeneous steel models with base diameter of 1.25 inches. Moderate and higher Mach numbers were obtained with one-inch diameter titanium-based models with hard copper noses. This combination was used to prevent excessive nose luminosity at higher velocities without encountering wall failure due to launch loads.

Sabots were constructed of lexan with integral dowels to hold the sabot halves in proper alignment. Two-piece steel pressure plates were used to distribute the load of the model base onto the sabot shoulder.

The models and sabots described were adequate to obtain data through the range of Mach numbers from 6.25 to 14. Attempts to extend the data to higher Mach numbers with copper and tungsten tipped models were unsuccessful due to failure or distortion of model tips during launch.

It will be shown later that model tip recession or changes in bluntness were small enough so that no appreciable effect on the data or results was experienced. It will also be shown in a later section that the exact location of transition does not affect the data. The optical data taken, however, were carefully examined for nose recession and to insure that transition was occurring close to the nose. Figures 2.3 and 2.4 are typical of the photographs taken during the test. On the original plates flow detail is much more distinct than that which appears in printed report figures. The shadowgraph of figure 2.3 must be closely examined to verify the location of transition close to the tip. On the schlieren of figure 2.4, however, (taken of the same model at a different station) the transition location is much more obvious. Both schlieren and shadowgraphs were taken of all launches.

Analysis of Data

The program under Task 2.0 was conducted primarily to obtain drag coefficients for a slender cone whose surface was almost entirely wetted with a turbulent boundary layer. In this case the contribution of the turbulent skin friction to the total drag will be relatively large and will permit some analysis of turbulent skin friction at high Mach numbers and low wall to stagnation temperature ratios. Most of the data reported were taken for that purpose. It was desired also to compare these data with several theoretical methods available for computing turbulent skin friction drag.

In order to perform these calculations it was necessary to know the location of boundary layer transition or transition Reynolds numbers over the range of Mach numbers being considered. To determine transition Reynolds numbers, a few launchings were conducted at lower Reynolds numbers such that transition occurred well back from the nose of the

model, generally between tne mid point and aft edge of the model surface. The manner in which these data were used will be discussed later in this task report.

The measured time-distance data from the twenty-seven spark shadowgraph stations along with the physical characteristics of the models were used with a standard ballistics range data reduction program to obtain drag coefficients. A description of this data reduction procedure is given in reference (2.1). This procedure involves fitting the time-distance data to a theoretical relation. The probable errors in the drag coefficients are based on the probable errors determined in fitting the theoretical relation. The drag coefficients and the probable errors for each successful launching are listed in Table 2.1. During its flight in the ballistics range, a model performs an oscillatory pitching motion as a function of time or downrange distance. This pitching motion is characterized for each launching by a value for the mean squared angle of attack, which is a time integrated average of the angle of attack of the model squared. For all except one launching, the mean squared angle of attack was only one degree or smaller. One launching at a Mach number of 6 and a Reynolds number of 3×10^6 had a mean squared angle of attack of 4 degrees squared. It has been assumed that the drag coefficient varies linearly with the mean squared angle of attack. That is,

$$C_D = C_{D_o} + k\,\overline{\alpha^2} \qquad (1)$$

The validity of this assumption is shown for instance in references (2.1) and (2.2). It was further shown in reference (2.1) that the slope k of the C_D versus α^2 curve is constant for a given configuration (i.e., independent of the free-stream Mach number and Reynolds number). Since the variation in α^2 was very small for any group of the present data, obtained at essentially fixed values of free-stream conditions, it was decided tc use the value of k obtained from the data presented in reference (2.2). These data were obtained from models of the same configuration as was used in the present tests. The value of k was 0.0012 per degree squared. It can be seen that the maximum correction made to any of the drag coefficients, except the one for the low Reynolds number condition, was less than 2 percent so

that the effect of any slight variation in k is negligible. All of the reported drag coefficients were reduced to equivalent zero angle of attack values using equation (1) and k equal to 0.0012 per degree squared. Values for α^2 and the zero angle of attack drag coefficient for each launching are listed in Table 2.1. Using the time-distance measurements, a mid-range velocity was determined for each launching. The mid-range Mach number was calculated using the values of the mid-range velocity and measurements of the temperature of the air in the range for each launching. A free-stream Reynolds number was computed using the mid-range velocity, temperature and pressure measurements for each launching, and the wetted length S for the cone. These quantities are listed in Tables 2.1 and 2.2.

The zero angle of attack drag coefficients have been plotted against the mid-range Mach number for each launching in figure 2.5. A smooth curve has been faired through these data. The repeatability of these data is illustrated in figure 2.5 where it is seen that no point deviates from this smooth curve by more than 3 percent. This deviation of 3 percent occurs for a few of the higher Mach number data points at the lowest value of drag coefficient. For the rest of the data between Mach numbers of approximately 6 to 9.5, the maximum deviation is about 1.5 percent. Although these tests were conducted at nominal values of Reynolds number, varying between 21 x 10^6 and 29 x 10^6, the effect of this variation of Reynolds number on the drag coefficients is negligible. In figure 2.6, data from the present tests at nominal Mach numbers of 9 and 13.3 have been used to extend the Reynolds number range of the data presented in reference (2.2). In addition, data from the present tests for a nominal Mach number of 6.1 are also presented. Theoretical curves have been calculated for each of the three Mach number conditions. The method used for calculating these curves will be discussed in the section on comparison of data with theory. It can be seen from figure 2.6 that the variation in the total drag coefficient for Reynolds numbers between 20 and 30 x 10^6 is less than 1.5 percent.

All of the models used in reference (2.2) and all but one model used in this present series of tests were designed and constructed such that they were hollow with open bases. To ascertain the effect of the open base on the base drag component and hence on the total drag coefficient, one launching was made with a model whose base had been closed

by fastening a plate across the aft end of the model. This model was launched at a Mach number of 8, and the resulting zero angle of attack drag coefficient is shown in figure 2.5 as a solid black circle. As can be seen, there was no measurable effect in the drag coefficient due to closing the base. Further, measurements of the base flow geometry made from shadowgraph photographs taken during the tests failed to reveal any measurable differences.

The total flight time for these tests varied from 84 milliseconds for the low Mach number tests to 37 milliseconds for the high Mach number tests. Because of these very short flight times it has been assumed that the wall temperature of the models remained at room temperature, which is equal to the free-stream range temperature reported in Table 2.2. Calculations of the wall temperatures of free-flight range models of the type used in these tests were made and reported in reference (2.2). These calculations showed that with the exception of the immediate nose region, the wall temperature of the model varied only slightly from room temperature. Using this assumption, the wall to stagnation temperature ratio associated with each particular Mach number has been calculated over the range of Mach numbers for which data are reported. The stagnation temperatures are based on equilibrium conditions for a real gas and were calculated using the charts in reference (2.3). The scale across the top of the graph in figure 2.5 represents those temperature ratios corresponding to the Mach number shown across the bottom of the graph.

Comparison of Data with Theory

The purpose of these tests was to obtain experimental hypersonic drag coefficients for a slender cone (almost entirely covered with a turbulent boundary layer) which could be used to check the validity of various applicable turbulent skin friction theories. In order for a comparison between data and theory to be meaningful, it was necessary that the configuration and test conditions used be such that the contribution of the turbulent skin friction drag coefficient be a significant portion of the total drag coefficient. A slender conical shape was chosen since this would minimize the pressure drag coefficient component and due to the large amount of wetted area, amplify the skin

friction drag coefficient component. Since high heating rates would be encountered at the high Mach numbers and high range pressures, it was necessary to slightly blunt the nose of the models to prevent or at least minimize melting and ablation of the tips of the models.

The pressure drag coefficient C_{D_P}, the friction drag coefficient C_{D_F}, and the base drag coefficient C_{D_B} (components of the total drag coefficient C_{D_o}) have been calculated over the range of free-stream Mach number for which data are presented. The results of these calculations are shown in figure 2.7. Also shown in figure 2.7 is the percent contribution to the total drag coefficient of each of these components. The laminar skin friction drag component is not shown since it was less than one percent of the total drag coefficient. This is true because transition was assumed to occur very near the nose for these calculations. The method used for making these calculations will be discussed later in this section. Although for all Mach numbers the pressure drag coefficient is a large component of the total drag coefficient (varying from 37.4 percent to 50.5 percent), it is considered that it can be calculated with the highest degree of accuracy. Unfortunately, for the lower values of Mach number the base drag coefficient is also a large component of the total drag coefficient, having a value of approximately 40 percent of the total drag coefficient at a Mach number of 6. However, this component rapidly decreases with increases in Mach number so that at Mach number 14 it is only 12 percent of the total drag coefficient.

Total drag coefficients were calculated for the test configuration and test conditions utilizing three different turbulent skin friction theories. These total drag calculations can then be compared with the experimentally measured total drag coefficients. The total drag coefficients were calculated by summing up computed values for the pressure drag coefficient, the friction drag coefficient due to laminar flow over a portion of the body, the friction drag coefficient due to turbulent flow over a portion of the body, and the base drag coefficient.

The pressure drag coefficient is obtained by integrating over the surface of the body the component (in the direction of the longitudinal axis) of the local force due to the static

pressure acting on the body. This resulting force is non-dimensionalized by the free-stream dynamic pressure and the base area of the cone. Since the bodies being considered are sphere-cone configurations, it is assumed that the static pressure from the tangent point to the base of the model is the pressure which results from inviscid flow over a sharp cone of the appropriate angle. The static pressure over the hemisphere nose portion of the body is taken as that predicted by modified Newtonian impact theory where the pressure coefficient is given as

$$C_p = C_{p_M} \sin^2 \theta$$

and C_{p_M} is the maximum pressure coefficient (i.e., that pressure coefficient occurring at the stagnation point). Although this is an extremely simple scheme for determining the pressure distribution over a sphere-cone configuration, it gives very good results particularly at high Mach numbers. To illustrate this point, the pressure distribution for a 10-degree half-angle cone flying at Mach number 20 was calculated by the method of characteristics and presented in reference (2.4). This pressure distribution is shown as the solid line in figure 2.8. Also shown in figure 2.8 as a dashed line is a pressure distribution computed using the modified Newtonian impact theory for the spherical portion of the body and inviscid sharp cone theory for the conical portion of the body. Comparing the two pressure distributions in figure 2.8, it is seen that after a distance of approximately 5 nose radii along the body the method of characteristics solution is equal to the inviscid sharp cone value. Further, the larger deviations in the two pressure distributions occur near the nose of the body where the surface area involved is a very small percentage of the total surface area. For this reason, using the simple scheme (Newtonian - inviscid sharp cone) mentioned previously produces a negligibly small error in the calculated pressure drag coefficient. Experimental data obtained and compared to Newtonian impact theory by Hastings and Chones (reference (2.5)) indicate that this method applied equally well at low Mach numbers.

The base drag coefficient is computed by assuming that the base pressure is constant over the base of the cone and equal to one-tenth of the free-stream static pressure.

Based on the work reported by Love (reference (2.6)) and also that reported by Whitfield and Potter (reference (2.7)), this assumption seems well justified.

The skin friction drag due to laminar flow over a portion of the body is calculated using the method formulated and reported by Wilson (reference (2.8)). This method permits values for the local skin friction coefficient to be calculated. Also, the various boundary layer thickness parameters can be calculated along the length of the cone. Further, properties just outside the boundary layer can be calculated. The method includes the effect of the slight blunting of the nose of the cone. The assumption is made that the flow just outside of the boundary layer is adiabatic, but it is not required to be isentropic. Once the distribution of skin friction coefficient along the surface of the body is obtained the integration of an appropriate component of the shear stress in the drag direction can be performed to obtain the laminar skin friction drag. This drag is then nondimensionalized by the free-stream dynamic pressure and the base area of the cone to obtain a laminar skin friction drag coefficient. The effect of nose bluntness was evaluated and can be seen in figure 2.9. The models used were manufactured with a nominal nose to base radius ratio of 0.03. Although the nose of the models was obscured in the shadowgraph pictures by the bow shock and some luminosity, an attempt was made to estimate the nose bluntness on downrange photos. For the highest Mach number case the upper limit was estimated less than 0.07. Referring to figure 2.9, it can be seen that a variation in bluntness ratio of 0.03 to 0.07 results in a variation of drag coefficient of only 1.25 percent. For the reasons discussed previously, it is considered that the actual variation in bluntness during these tests was less than this. It is also apparent from figure 2.9 that variation in nose bluntness due to fabrication tolerances as indicated in Table 2.1 should have a negligible effect on experimental results.

Wilson has derived a similar method (reference (2.9)) to that just described for calculating turbulent boundary layer characteristics for slightly blunted slender cones. Values for the local flow properties just outside the boundary layer are also obtained. Both the laminar and turbulent method are momentum-integral methods and are such that any flat plate relation of C_f vs R_ϑ can be used to perform the calculations. It is also necessary to specify

relations for the shape parameter, H, and the thickness parameter δ/θ. As explained for the laminar drag, once the distribution of turbulent skin friction coefficients is obtained along the length of the cone, then a value for the turbulent skin friction drag coefficient can be obtained.

The methods just discussed for computing the various drag coefficient components have all been integrated into a computer program for computing the total drag coefficient for a slightly blunted slender cone. This program has been coded for use in a high-speed digital computer. The program starts calculating using laminar boundary layer equations. At some arbitrary predetermined transition Reynolds number, the program then switches to turbulent boundary layer equations. To better establish the relation between Mach number and transition Reynolds number, several launches were made at various Mach numbers with the range pressure at values that located transition roughly halfway back on the cone surface. At this location, transition is readily observed in the shadowgraph photos. The results of these firings are indicated in figure 2.10. Calculations were made to determine the sensitivity of drag coefficient to fluctuations in transition location. The maximum variation in drag coefficient for a fluctuation of one inch in transition location when transition is close to the nose is 0.9 percent. It appears, therefore, that knowledge of the exact location of transition on the model is not critical. Several different total drag coefficients have been calculated over the range of test conditions for which data are presented. These different total drag coefficients were calculated using identical equations for all of the components except for the turbulent skin friction drag coefficient. For the several different cases the turbulent skin friction drag coefficient was calculated as described using the turbulent boundary layer characteristics associated with several theoretical methods. These methods and the equations used for determination of the turbulent skin friction are found in references (2.9) through (2.11). The results are summarized in figure 2.11.

The overall accuracy of the data as shown in this figure is not great enough to differentiate between theories such as Wilson's and some similar methods. The difference between the data and the other theories shown is significant, however. The agreement with experiment for Wilson's method is quite good for Mach numbers between 6 and 8.5 at higher

Mach numbers, however, the theory appears to predict a higher value of drag coefficient than observed. Although the theories of Fenter and Winkler and Cha predict a considerably lower value of drag coefficient than experiment through the entire Mach number range investigated, the trend of the variation in drag with Mach number is very close to that indicated by the data. This leads one to contemplate some adjustment factor or constant that would bring the theory and experiment together for these cones. The data shown represent values of wall to stagnation temperature ratio as indicated in figure 2.5 and, therefore, represent only a small section of data that would be represented by a family of curves of several values of constant T_w/T_∞

There is a need for more thorough evaluation of theory and for more experimental data at other conditions. The present experimental information fills in a small part, however, of an area in which good data have been almost nonexistent.

References

(2.1) Lyons, W. C., Jr., Brady, J. J., and Levensteins, Z. J., "Hypersonic Drag, Stability, and Wake Data for Cones and Spheres," Presented at AIAA Aerospace Sciences Meeting Jan 1964, Preprint No. 64-44.

(2.2) Sheetz, N. W., Jr., "Free-Flight Boundary Layer Transition Investigations at Hypersonic Speeds," Presented at AIAA Second Aerospace Sciences Meeting Jan 1965, AIAA Paper No. 65-127.

(2.3) Feldman, S., "Hypersonic Gas Dynamic Charts for Equilibrium Air," Avco Research Laboratory Jan 1957.

(2.4) Ellett, D. M., "Pressure Distributions on Sphere Cones," Sandia Corp. Research Report SC-RR-64-1796, Jan 1965.

(2.5) Hastings, S. M., and Chones, A. J., "Supersonic Aerodynamic Heating of a Yawed Sphere-Cone Wind Tunnel Model," U. S. Naval Ordnance Laboratory, NavOrd Report 6812, Nov 1960.

(2.6) Love, E. S., "Base Pressure at Supersonic Speeds on Two-Dimensional Airfoils and on Bodies of Revolution With and Without Fins Having Turbulent Boundary Layers," NACA TN 3819, Jan 1957.

(2.7) Whitfield, J. D., and Potter, J. L., "On Base Pressure at High Reynolds Numbers and Hypersonic Mach Numbers," AEDC-TN-60-61, Mar 1960.

(2.8) Wilson, R. E., "Laminar Boundary-Layer Growth on Slightly Blunted Cones at Hypersonic Speeds," AIAA Journal of Spacecraft and Rockets, Jul-Aug 1965.

(2.9) Wilson, R. E., "Laminar and Turbulent Boundary Layers on Slightly Blunted Cones at Hypersonic Speeds," AGARDograph No. 97, May 1965.

(2.10) Winkler, E. M., and Cha, M. H., "Investigation of Flat Plate Hypersonic Turbulent Boundary Layers With Heat Transfer at a Mach Number of 5.2," U. S. Naval Ordnance Laboratory, NavOrd Report 6631, Sep 1959.

(2.11) Fenter, F. W., "The Turbulent Boundary Layer on Uniformly Rough Surfaces at Supersonic Speeds," Vought Research Center, Chance Vought Aircraft Inc., Report No. RE-E9R-2, Dec 1959.

TABLE 2.1 MODEL SPECIFICATIONS

Shot No.	Diam. B (in.)	Length Axial L (in.)	CG_N (%)	Weight (gm.)	Transverse I (gm. in.^{2})	Cone ½∢ (deg.)	Mtrl. N-B	Wetted Length S	R_N/R_B
752	1.000	4.398	56.3	42.3510	49.620	6.3	Cu Ti	4.421	.036
711	1.250	5.510	57.1	92.8208	145.51	6.3	Steel	5.553	.030
742	1.251	5.508	57.0	92.5440	145.04	6.3	Steel	5.572	.027
708	1.252	5.510	57.1	93.7180	147.48	6.3	Steel	5.569	.029
701	1.250	5.510	57.2	93.1762	146.62	6.3	Steel	5.584	.026
698	1.248	5.508	56.9	91.5295	143.97	6.3	Steel	5.551	.029
754*	1.240	5.491	60.8	100.6492	187.51	6.3	Steel	5.505	.029
700	1.250	5.509	57.1	93.0265	146.28	6.3	Steel	5.553	.030
702	1.251	5.509	57.2	93.6679	147.57	6.3	Steel	5.572	.027
710	1.250	5.509	57.1	93.2959	146.70	6.3	Steel	5.575	.026
715	1.000	4.400	56.0	42.3000	49.272	6.3	Cu Ti	4.413	.038
704	1.000	4.399	56.3	42.5819	49.900	6.3	Cu Ti	4.421	.036
796	1.000	4.406	57.6	43.3382	49.221	6.3	Cu Ti	4.458	.026
725	1.001	4.406	56.0	42.5421	49.557	6.3	Cu Ti	4.418	.038
749	1.000	4.406	56.0	41.5775	48.309	6.3	Cu Ti	4.421	.036
734	1.251	5.507	57.1	93.6740	147.29	6.3	Steel	5.564	.029
731	1.250	5.511	57.0	92.5220	144.86	6.3	Steel	5.568	.027

*has a base plate

N = Nose
B = Base

TABLE 2.2 EXPERIMENTAL DATA

Shot No.	M	V_∞ (fps)	P_∞ (atm.)	R_{∞_L} x 10^{-6}	$\overline{\alpha^2}$ (deg.^{2})	T_∞ ($^\circ$F)	C_D	Prob. Error	C_{D_o}
752	6.22	7048	.588	9.20	2.0	69.8	.0879	.0001	.0855
711	6.71	7621	.979	20.7	1.0	72.3	.0803	.0001	.0791
742	6.76	7666	.992	21.3	1.0	69.9	.0810	.0001	.0798
708	7.54	8566	.989	23.5	1.0	71.8	.0816	.0009	.0804
701	7.81	8877	.976	24.0	0.4	72.6	.0711	.0001	.0706
698	7.94	9016	.962	24.0	0.3	72.5	.0710	.0002	.0706
754	8.02	9096	.986	24.9	1.0	71.2	.0699	.0001	.0687
700	8.08	9184	.982	25.0	0.5	72.3	.0699	.0001	.0693
702	9.47	10757	.972	29.0	1.0	72.8	.0628	.0001	.0616
710	9.53	10844	.989	29.6	0.4	74.0	.0620	.0001	.0615
715	9.59	10896	.989	23.8	1.0	72.8	.0614	.0001	.0602
704	13.10	14873	.973	32.1	6.0	71.9	.051	.002	.0503
796	13.52	15488	.656	21.9	1.0	81.2	.0530	.003	.0518
725	14.14	16070	.652	23.1	1.0	73.2	.0537	.0005	.0525
749	6.03	6823	.391	5.97	4.0	69.0	.0801	.0002	.0753
734	8.34	9448	.324	8.58	2.0	70.1	.0648	.0003	.0624
731	8.52	9657	.260	7.00	8.0	70.3	.0669	.0003	.0573

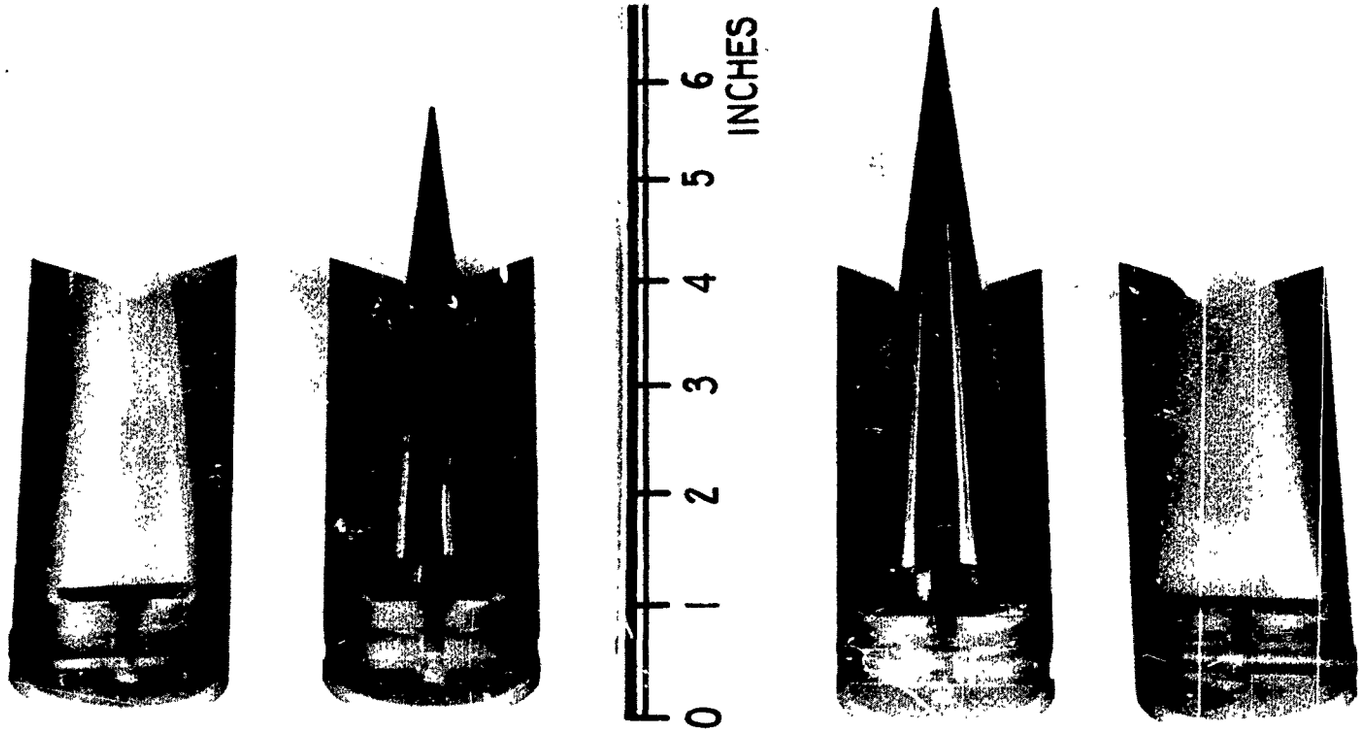

FIG. 2.1 MODEL AND SABOT CONFIGURATIONS FOR INTERMEDIATE (LEFT) AND LOW (RIGHT) MACH NUMBER PHASES

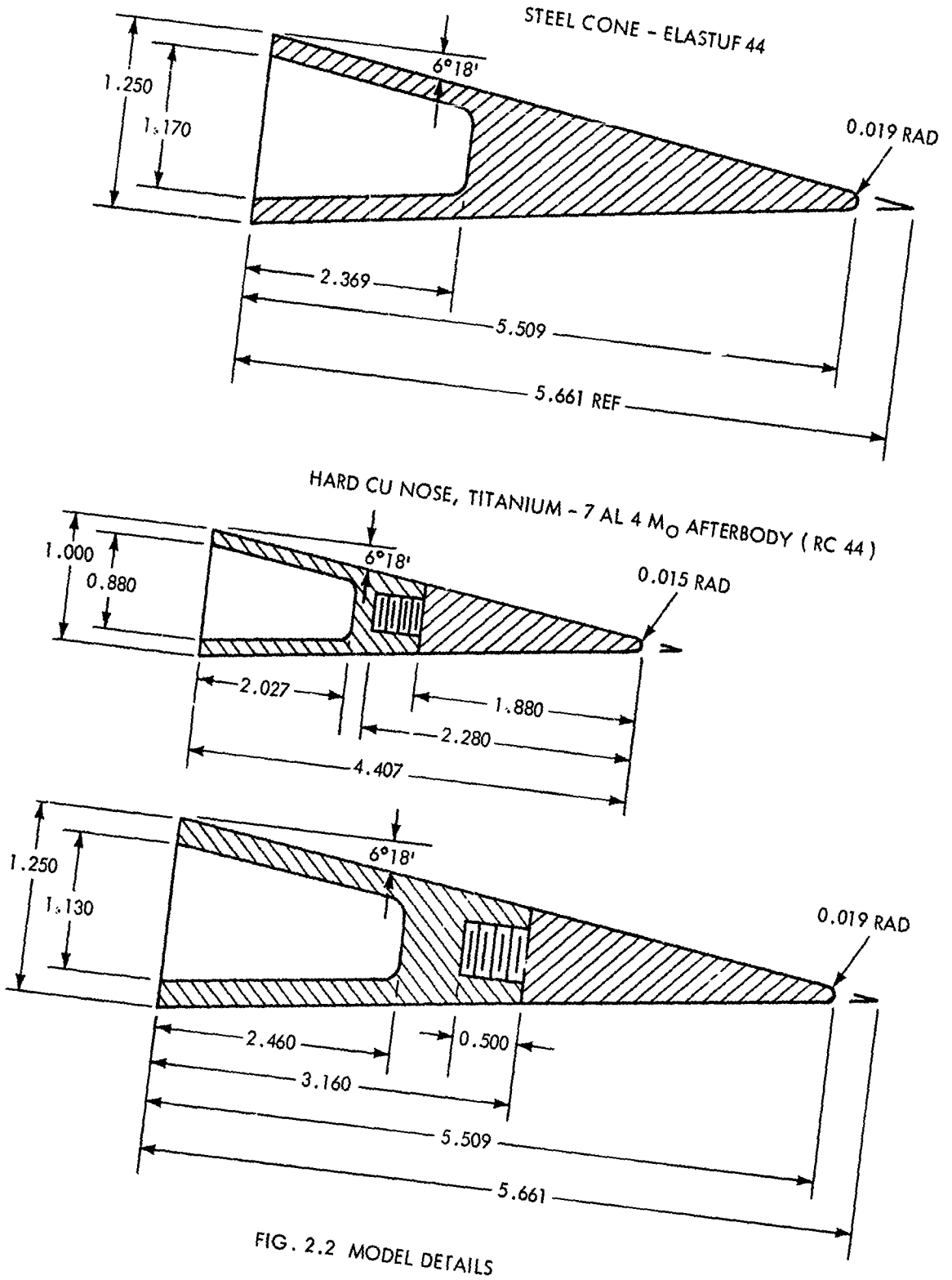

FIG. 2.2 MODEL DETAILS

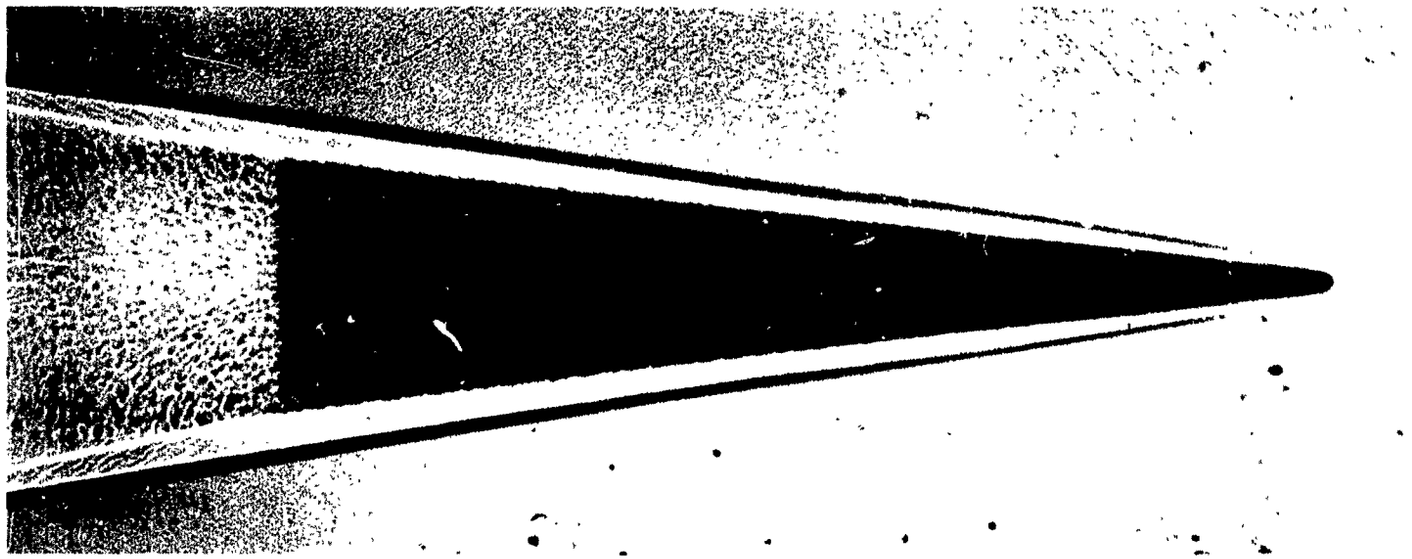

FIG. 2.3 SHADOWGRAPH OF MODEL FLYING AT STATION 360. MACH NUMBER 9.53 SHOT NO. 710.

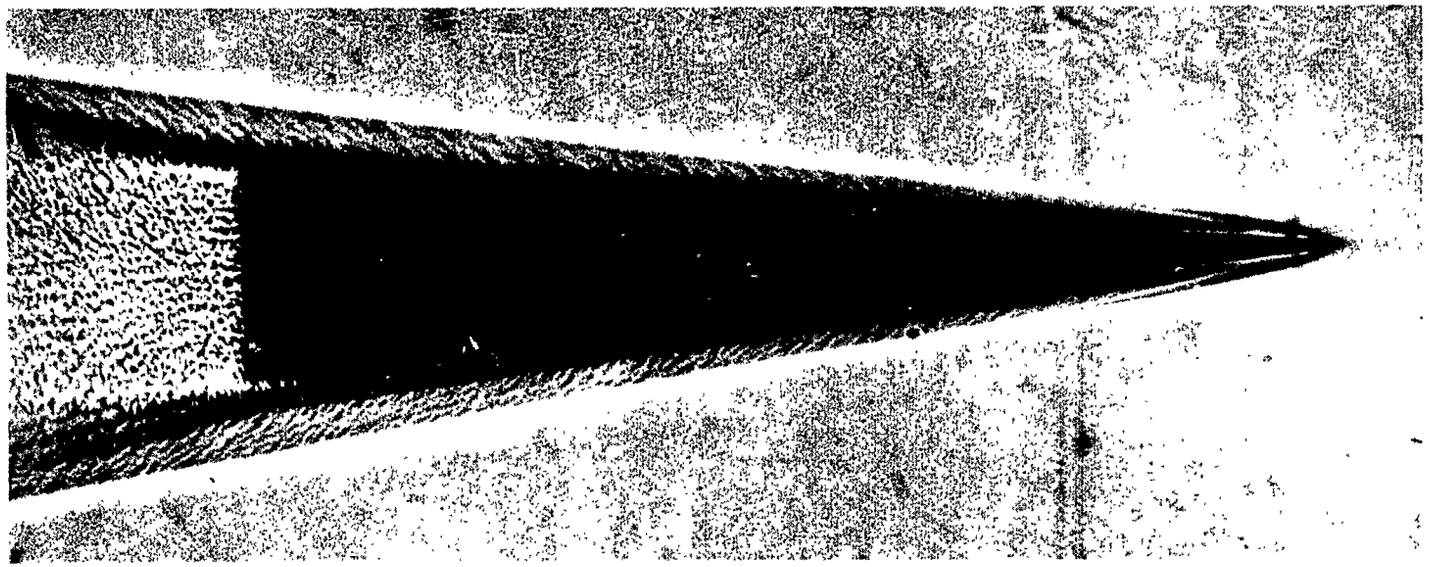

FIG. 2.4 SCHLIEREN OF MODEL FLYING AT STATION 245. MACH NUMBER 9.53 SHOT NO. 710.

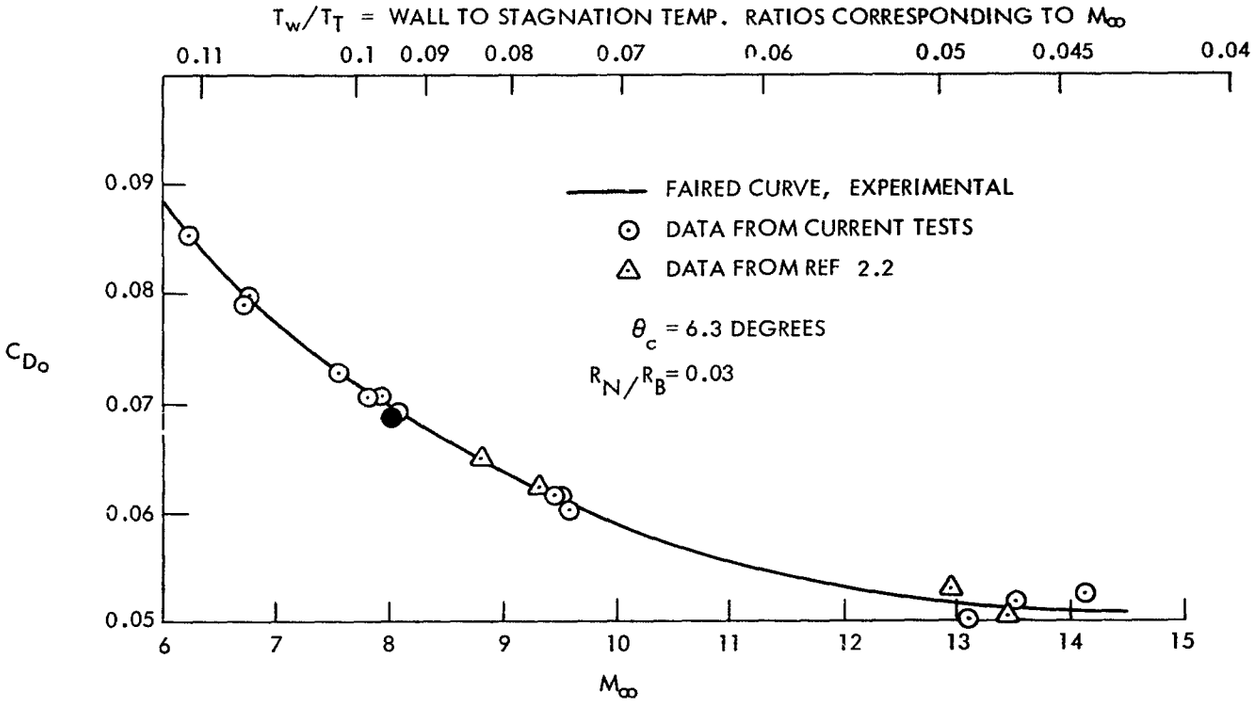

FIG. 2.5 MEASURED TOTAL DRAG COEFFICIENTS FOR A SLIGHTLY BLUNTED SLENDER CONE

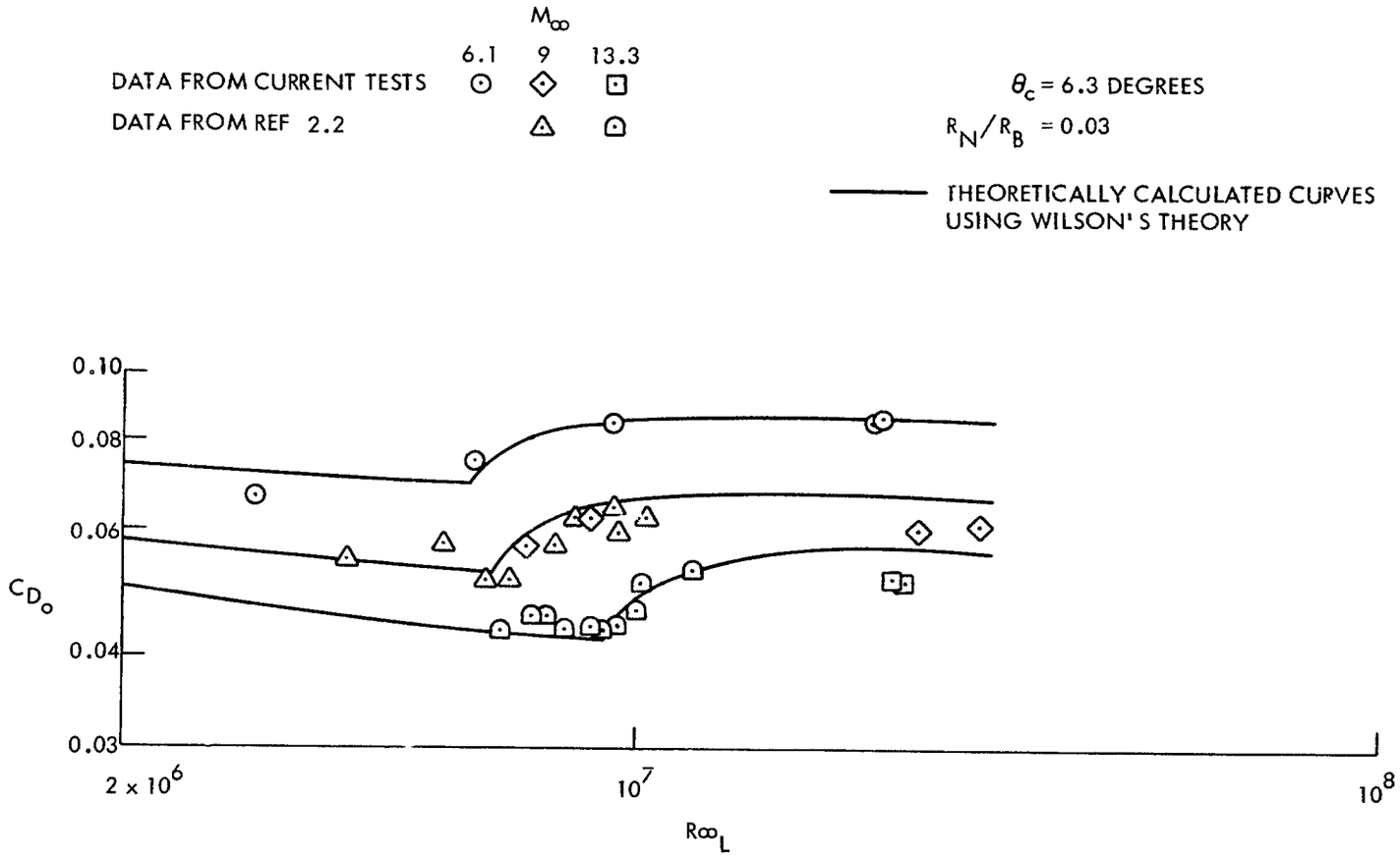

FIG. 2.6 VARIATION OF TOTAL DRAG COEFFICIENT WITH REYNCLDS NUMBER FOR A SLIGHTLY BLUNTED SLENDER CONE

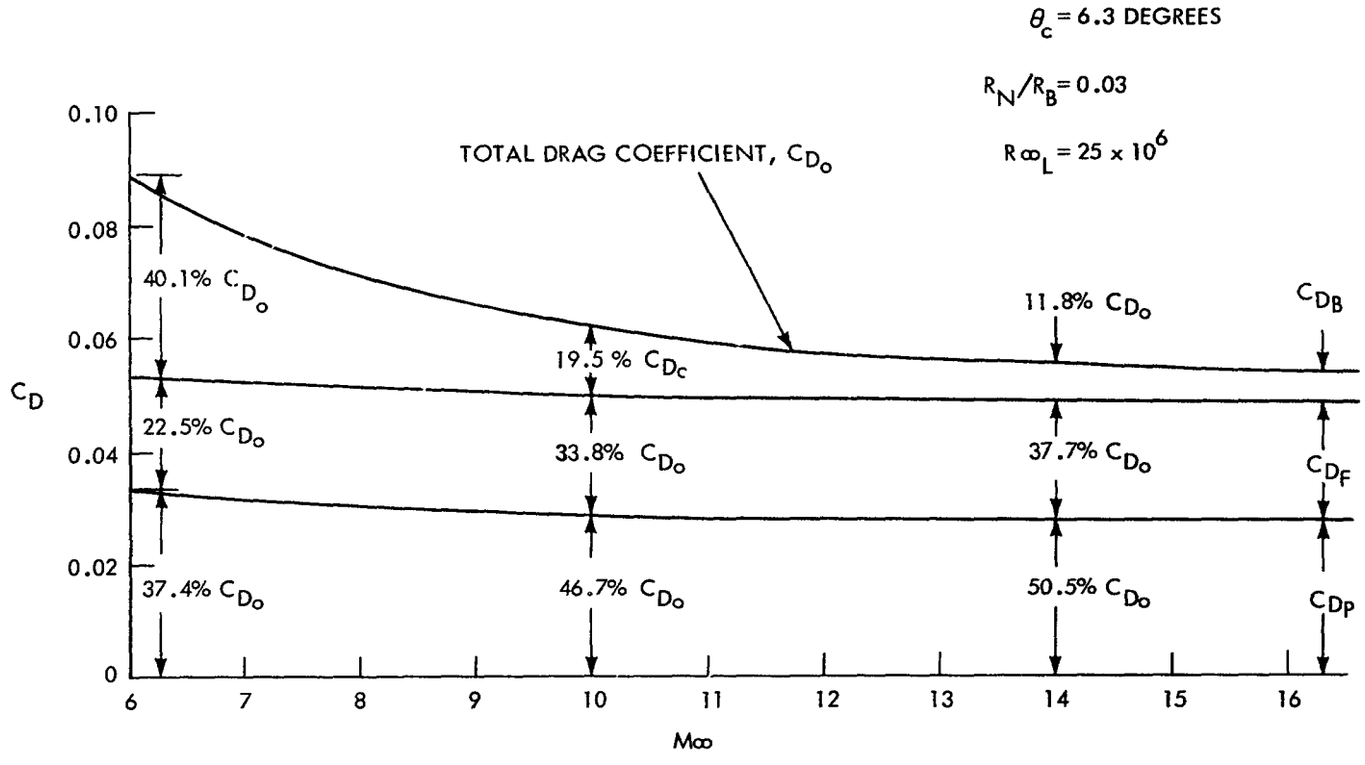

FIG. 2.7 CONTRIBUTION OF THE COMPONENTS OF THE TOTAL DRAG COEFFICIENTS FOR A SLENDER CONE

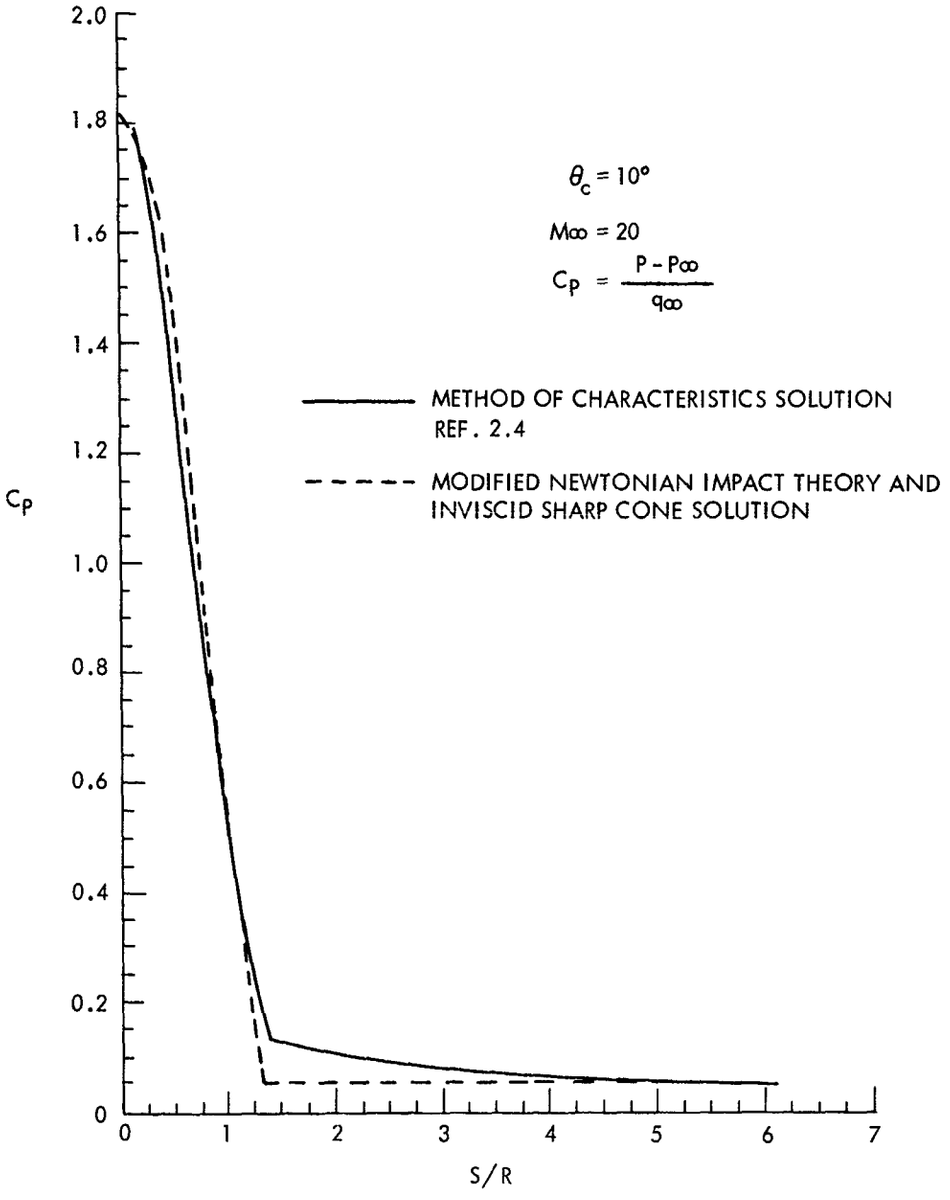

FIG. 2.8 PRESSURE DISTRIBUTION OVER SLENDER CONE

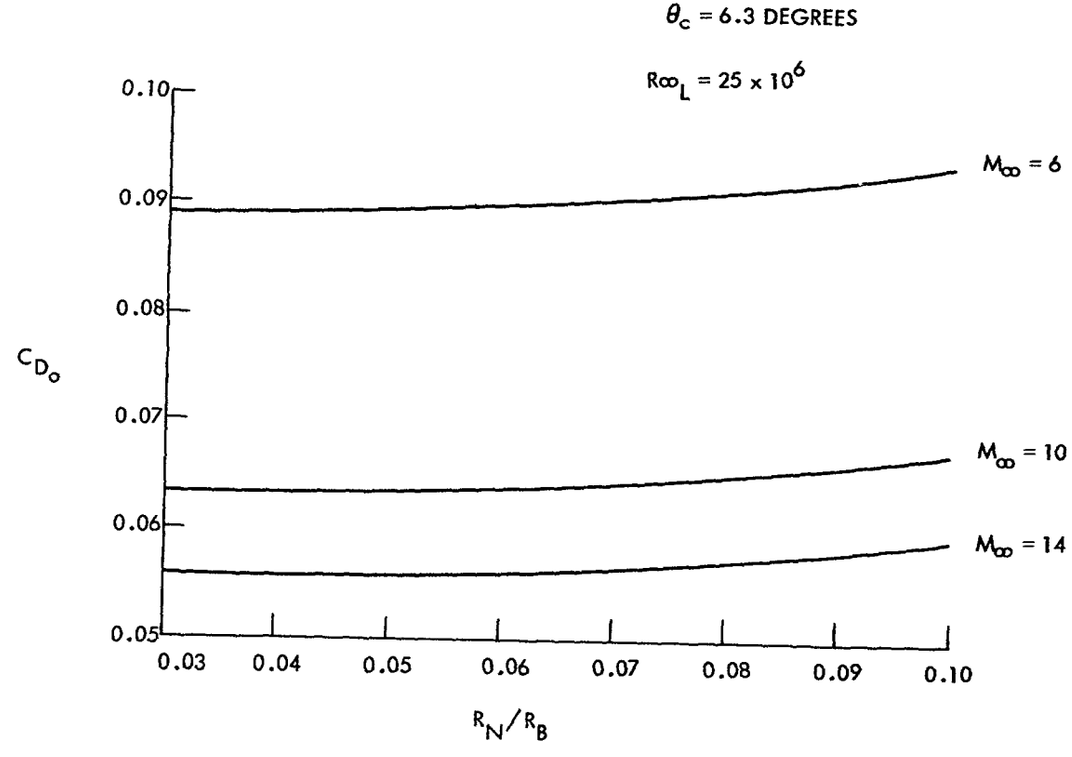

FIG. 2.9 EFFECT OF NOSE BLUNTNESS ON THE TOTAL DRAG COEFFICIENT FOR A SLIGHTLY BLUNTED SLENDER CONE

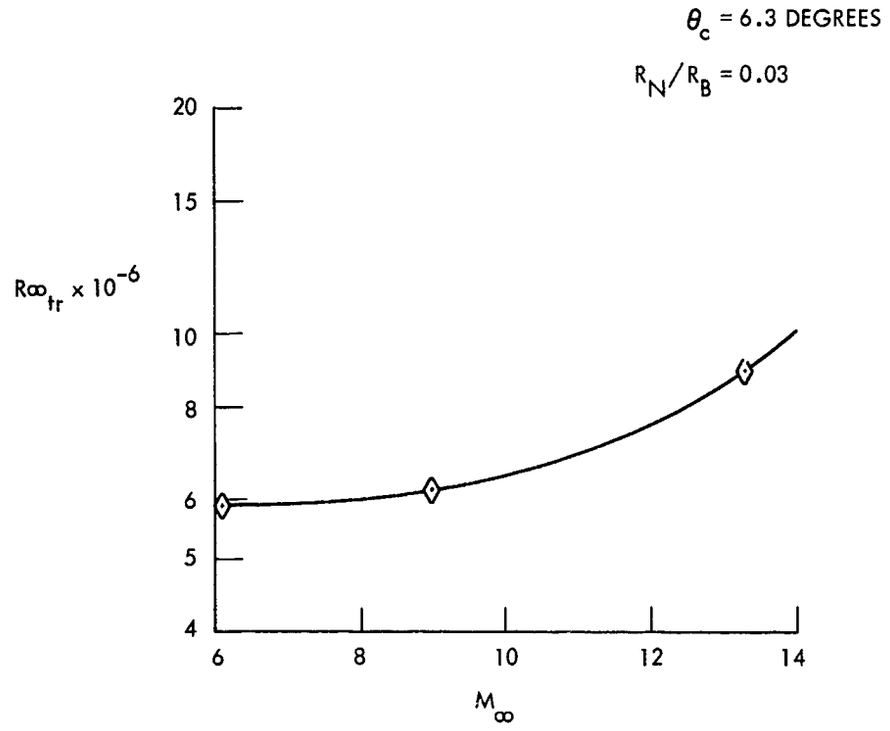

FIG. 2.10 VARIATION OF FREE STREAM TRANSITION REYNOLDS NUMBER WITH MACH NUMBER FOR A SLIGHTLY BLUNTED SLENDER CONE.

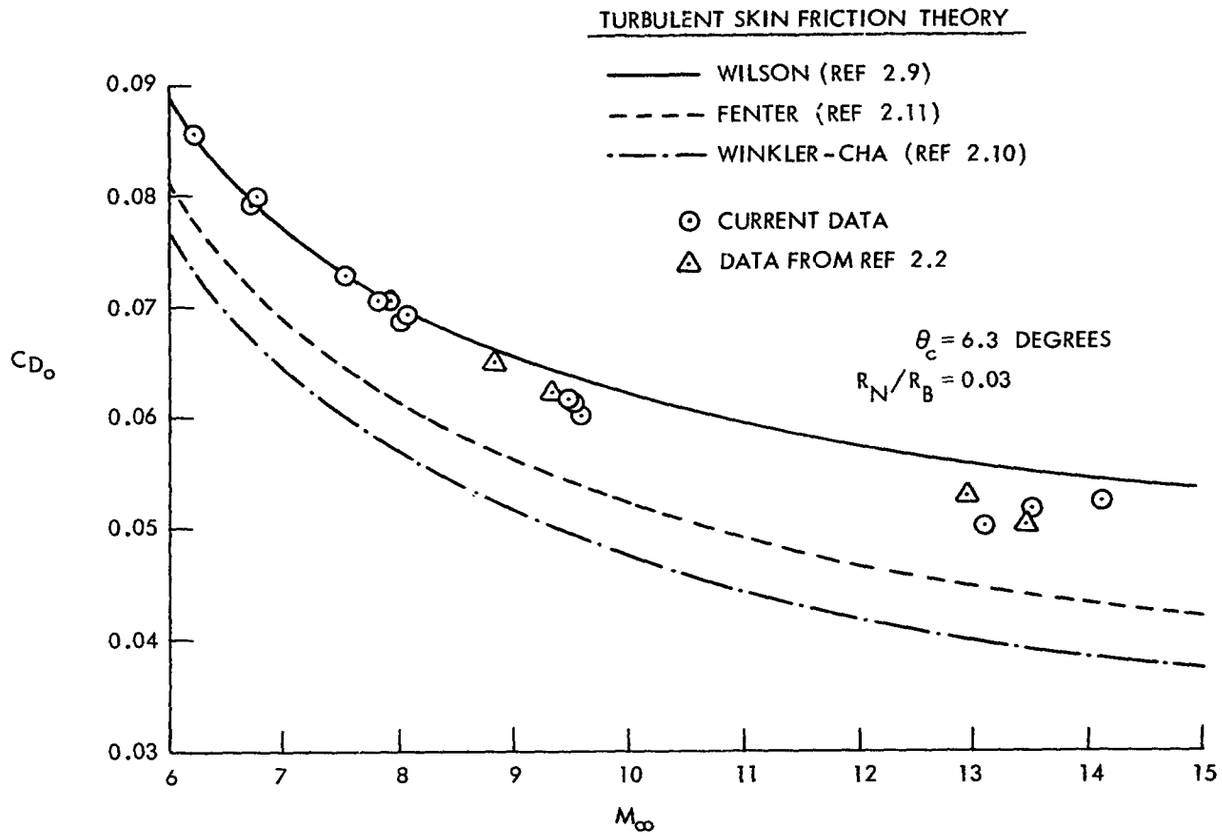

FIG. 2.11 COMPARISON OF THEORY AND EXPERIMENT TOTAL DRAG COEFFICIENTS FOR A SLIGHTLY BLUNTED SLENDER CONE

TASK 3.0

EFFECT OF HIGH HEAT TRANSFER RATES ON BOUNDARY LAYER TRANSITION

Introduction

Boundary layer transition has been of great interest to both the theoretician and the experimentalist. This interest is kindled by the importance of the nature of the boundary layer in a wide variety of aerodynamic problems. The magnitude of drag forces depends upon whether the boundary layer is laminar or turbulent. The aerodynamic heating rate is strongly influenced by the nature of the boundary layer. Other important phenomena that are affected by the location of boundary layer transition include the mass injection rate in boundary layer cooling systems, the location of the boundary layer separation point, and the structure of the wake.

A great deal of effort has been made to theoretically predict the boundary layer transition Reynolds number for a number of situations. However, a theoretical analysis that includes all of the parameters that affect the stability of the boundary layer would be extremely difficult, if not impossible. These parameters include Mach number, surface roughness, nose or leading edge bluntness, heat transfer rate, and pressure gradient. One of the most influential parameters on the location of transition, and one of the most controversial, is the effect of heat transfer rate. A theoretical study of a compressible boundary layer by Lees (reference (3.1)) indicated that a stabilizing effect on the boundary layer is produced by increasing the rate of heat transfer from the fluid to the body. This result has been generally accepted in certain flow regimes. In addition, it was suggested in reference (3.1) that at certain Mach numbers the laminar boundary layer can be completely stabilized by the presence of an appropriate amount of cooling of the boundary layer regardless of the Reynolds number. A large amount of experimental evidence substantiated this predicted stabilizing effect for moderate rates

of cooling. However, some more recent experiments (references (3.2), (3.3), and (3.4)) have indicated that this stabilizing effect does not exist at extremely high rates of heat transfer. In these experiments, it was observed that for certain test conditions increasing the heat transfer rate produced a destabilizing effect on the boundary layer. This destabilizing trend, "transition reversal," could not be satisfactorily explained by the early stability theories.

In a recent theoretical investigation, Reshotko (reference (3.5)) has recalculated the temperature ratios required to completely stabilize the boundary layer by considering the hitherto neglected temperature fluctuations and thermal boundary conditions. The recalculated values show that there are two loops of complete stability in the usual diagram of temperature ratio vs free-stream Mach number. The trends suggested by the two loops of complete stability tend to substantiate the experimentally observed transition reversal phenomenon.

Recent experimental programs have been conducted in the ballistics ranges at NOL to determine the effects of high rates of heat transfer on boundary layer transition. These tests have shown a very complicated dependency of the boundary layer transition Reynolds number on the ratio of the wall temperature to the recovery temperature. The tests were conducted on a sharp 5-degree half-angle cone at nominal Mach numbers of 3 and 5. The results have been reported in references (3.6) and (3.7). This task of the current ABRES program was planned to investigate these phenomena at a higher Mach number of 8. At the present time, there is no theoretical information available from which the stability of the boundary layer can be accurately predicted for these flow conditions. In addition, available experimental data in this area are not adequate.

Description of Tests

The current tests were conducted in the Pressurized Ballistics Range at NOL. A general description of the range can be found in Tables 1.2 and 1.3 of this report. In order to vary the ambient temperature and thus the temperature

ratio, an 18-foot section of the range was equipped with an electrical heater. The heater was capable of varying the ambient temperature in the range from approximately 80°F to over 800°F. The interior cross section was approximately one foot square. There were four vertical and four horizontal data stations located along the length of the heater at which spark shadowgraph photographs were taken of the model in flight. The heater was equipped with thermal shields at the data stations which protected the film emulsion on the photographic plates until approximately 20 seconds prior to launching the model. There were also doors on both ends of the heater that contained the heat within the box. These doors remained closed until approximately one second before launching. A photograph of the heater prior to installation in the range is shown in figure 3.1.

The basic test configuration was a sharp 5-degree half-angle cone with a finned cylindrical afterbody to increase the stability and decrease the angle of attack. This was essential since it is extremely difficult to analyze the effect of angle of attack on boundary layer transition. It was desirable to make the models as large as possible to provide a long surface for boundary layer observations. The final size was limited, however, by the capabilities of the launcher. At the lower test velocities, it was possible to use a model with a base diameter of 0.8 inch. However, at the higher test velocities it was necessary to reduce this to 0.5 inch. A photograph of a typical model and sabot is shown in figure 3.2.

Extreme care was taken to obtain and preserve both a smooth surface and a sharp tip on the models prior to launching. The models were constructed of tool steel and titanium. The surface was finished by grinding. It was found that center line average surface finishes of one to 6 microinches root-mean-square could be obtained consistently by this method and that further attempts to improve the surface by polishing only resulted in introducing waviness in the surface. The surface finish was measured with a Taylor-Hobson "Talysurf" recorder. No attempt was made to produce a radius on the tip of the models. The tips were ground as sharp as possible and inspected under magnification immediately prior to launching. Models with bent or broken tips were discarded.

The heat transfer rate was varied by adjusting the ambient air temperature in the heated section of the range. The launch velocity was varied with the range temperature to obtain the desired test Mach number. This was necessary because of the variation of the speed of sound with temperature. After the desired range temperature and Mach number had been chosen, the range pressure was adjusted to produce the required Reynolds number. The transition Reynolds number was obtained by measuring the flow properties such as velocity, temperature, pressure, and length of laminar flow in the boundary layer. The length of laminar flow was obtained from shadowgraph photographs taken of the model in free flight. The photographs have sufficient clarity and detail that accurate estimates can be made of the transition location.

Data Reduction Procedures

The basic data are reduced to a local transition Reynolds number based on the local flow conditions and the length of laminar flow on the body. In order to obtain the local flow properties, it is first necessary to determine the free-stream conditions. The range pressure is measured directly by pressure gages. The free-stream velocity is determined at each data station by measuring the time required for the model to travel from one data station to the next. Two thermocouples are located at each data station within the heated section of the range to measure the ambient temperature at the stations. The free-stream density can be calculated from the equation of state since both the pressure and temperature are known. Using these free-stream conditions, the corresponding local properties can be calculated with the aid of tables of flow properties for yawed cones (reference (3.8)) and tables of isentropic flow (reference (3.9)). Two rays of the boundary layer can be seen on each shadowgraph, one on the windward surface of the model and one on the leeward surface. In general, the model is at some angle of attack to the free stream. In order to obtain the local flow properties along each ray, the angular orientation of the ray with respect to the pitching plane is determined from the horizontal and vertical components of the angle of attack. After the orientation of the ray has been determined, the local flow conditions are determined from references (3.8) and (3.9).

The location of boundary layer transition is determined optically from the spark shadowgraph photos taken of the model during its flight down the range. The photographic plates used in these tests consist of film emulsion on 14 x 17 inch glass plates. Photographs are obtained of the model at each data station. The location of transition is measured from the tip of the image directly from the glass photographic plate. Examples of the shadowgraphs obtained in this program are shown in figures 3.3 and 3.4. It should be noted that in figure 3.3 the model is at a very low angle of attack and at this condition the location of transition is approximately the same distance back from the tip on both the top and bottom rays. However, in figure 3.4 where the model is at a larger angle of attack, it can be seen that the length of laminar flow on the windward ray is more than double the length of laminar flow on the leeward ray. This illustrates the need for maintaining very low angles of attack.

The Reynolds number based on the momentum thickness and local flow properties at the location of transition was also calculated. By applying Mangler's transformation to flow over a flat plate, it can be shown that the boundary layer momentum thickness for a flat plate is 3 times the momentum thickness obtained on a cone at the same local Mach number, local Reynolds number, and wall to local temperature ratio. The flat plate momentum thickness is given by

$$\theta_{\text{flat plate}} = \frac{C_F}{2} x$$

The above equation is obtained by integrating the momentum equation. The laminar value of the mean skin friction coefficient was obtained from reference (3.10).

In addition to determining the local flow conditions over the surface of the model, calculations were made to estimate the temperature rise of the surface during the flight. In order to make the calculations, the model was divided into sections along the body. Each section was treated as a semi-infinite slab and the heat transfer rate into the section was calculated from the average local flow properties over the section. In view of the short flight time involved, the model selected for the calculations is considered to be

a reasonable choice. The results of a typical calculation are shown in figure 3.5. From figure 3.5, it can be seen that except for the immediate area of the tip of the model the surface temperature increases only slightly during the test. The temperature rise of the model is limited by the short time required for the model to travel through the range at the test Mach numbers.

Discussion of Results

Successful launchings were made at ambient range temperatures of approximately 80°F, 200°F, and 400°F. These correspond to ratios of wall temperature to recovery temperature of approximately 0.09, 0.08, and 0.05, respectively. Local transition Reynolds numbers have been calculated for these launchings based on the calculated local flow properties and the length of laminar flow as measured from the shadowgraph. Figure 3.6 shows the variation of the local transition Reynolds number with the ratio of the wall to recovery temperature ratio. Data obtained from earlier tests at NOL at Mach numbers of 3 and 5 are also presented in figure 3.6. The data points marked by an arrow indicate launchings for which the boundary layer remained completely laminar. In these cases "minimum transition Reynolds numbers" were calculated and presented based on the length of the model. The model configuration for the Mach number 3 and 5 tests was the same as that used in the present tests (sharp, 5-degree half-angle cone). The test conditions and transition measurements for the Mach number 5 and 8 tests are presented in Tables 3.1 and 3.2. Similar data for the Mach number 3 tests are presented in reference (3.7).

It should be noted from the data presented in figure 3.6 that while transition reversal was observed at all three Mach numbers, an additional effect was noted in the Mach number 5 tests. At temperature ratios below approximately 0.12, further decreases in the temperature ratio had a stabilizing effect or "double reversal effect" similar to that observed by Wisniewski and Jack in a wind tunnel experiment reported in reference (3.11). However, the double reversal observed in the wind tunnel occurred at a considerably higher temperature ratio.

Although the data obtained at Mach number 8 show, in general, a transition reversal trend, a suggestion of an impending double reversal trend at lower temperature ratios is given by one of the launchings at a temperature ratio of approximately 0.05. The boundary layer remained entirely laminar over the conical surface for this launching which was made at the lowest temperature ratio investigated. For this launching, a minimum transition Reynolds number of approximately 5.7×10^6 was calculated based on the length of the conical surface. This value is indicated by an arrow in figure 3.6. During another launching at essentially the same temperature ratio, transition occurred at a considerably lower Reynolds number, 4.6×10^6. The same variation in transition Reynolds number between launchings at the same, or nearly the same, temperature ratio was observed in the Mach number 5 tests in going from the transition reversal region to the double reversal region. Attempts made to obtain data at lower temperature ratios were unsuccessful. Improvements in technique to eliminate this problem in future tests will be discussed later.

It is interesting to note that while the original theoretical stability analysis of a compressible boundary layer by Lees (reference (3.1)) cannot explain the existence of a transition reversal region, the more recent analysis by Reshotko (reference (3.5)) can at least qualitatively explain both the transition reversal and the double reversal region. The calculations of Reshotko show that there are two loops of complete stability in the usual diagram of temperature ratio vs free-stream Mach number. By decreasing the temperature ratio while holding the Mach number constant, it is possible to first stabilize the boundary layer as you approach and move into one of the theoretical stability loops. However, as the temperature ratio is decreased to move out of the first stability loop, the boundary layer is destabilized. This is characteristic of the transition reversal region. Finally, as the temperature ratio is decreased even further, a second stability loop is approached and again the boundary layer is stabilized. This is characteristic of the double reversal region.

In addition to calculating transition Reynolds numbers based on the length of laminar flow, Reynolds numbers were calculated for each launching based on the momentum thickness at the location of transition and the local flow properties. The results of these calculations are shown in figure 3.7.

These data also show the same transition reversal trend as was observed in figure 3.6. Calculations were not made for launchings in which the boundary layer remained laminar over the entire body.

The current tests indicate the possibility of an impending stabilizing effect on the boundary layer at the lowest temperature ratio investigated. Attempts were made to obtain data at lower temperature ratios to investigate this possibility, but excess model luminosity darkened the photographic plates and it was not possible to observe the boundary layer. In order to obtain lower temperature ratio, both the range temperature and velocity had to be increased. This increased the aerodynamic heating input to the thin titanium fins sufficiently to cause the fins to glow.

It was possible to verify the source of the luminosity by monitoring the light intensity with a photoelectric pickup as the model passed a data station. A typical oscilloscope record of the variation in the light intensity is presented in figure 3.8. A movement along the curve from the left to the right represents an increase in time while a downward displacement of the curve represents an increase in light intensity. An increase in light intensity produces an increase in voltage generated at the photoelectric pickup. The intensity level of the light screen used to trigger the photographic station upon arrival of the model is shown by the initially horizontal portion of the curve. After approximately 900 microseconds, there is a slight increase in intensity as the tip of the model begins to move in front of the pickup. As the glowing tip moves past the pickup, the intensity decreases indicating the presence of the cooler body which is not luminous. After a sufficient time interval to allow the fins to move in front of the pickup, however, the intensity increases drastically indicating that the fins are glowing very brightly.

Two steps have been taken to solve the problem of excessive model luminosity. First, a preliminary design of a modified range model has been made that will reduce the amount of luminosity. A sketch of the modified range model is presented in figure 3.9. The model still has the same basic external configuration, i.e., a sharp, 5-degree half-angle cone with a finned afterbody. However, a number of improvements have been incorporated into the new design.

The conical surface will be coated to reduce any luminosity originating from that area. Also, both the fin material and thickness will be changed to reduce fin luminosity.

In addition to modifying the range model to reduce the level of luminosity produced by the model, new photographic stations have been designed for the Pressurized Ballistics Range that will be less sensitive to luminosity originating from the model surface. The system presently in use is a divergent source spark shadowgraph that is extremely sensitive to light originating anywhere within view of the photographic plate. The new photographic stations use a focused shadowgraph system that is less sensitive to luminosity that does not originate at the spark source. Therefore, the unfavorable effect of model luminosity should be reduced with the new system.

Summary of Data

Transition Reynolds numbers have been experimentally obtained on a sharp, 5-degree half-angle cone. These tests were conducted at a Mach number of 8 and over a range in the ratio of wall temperature to recovery temperature of 0.05 to 0.09. Reynolds numbers based on the momentum thickness and local flow properties at the location of transition were calculated for each launching in which transition occurred on the body. The data were compared with previous data obtained at lower Mach numbers. While, in general, the data show a destabilizing effect on the boundary layer of decreasing the temperature ratio, there is some evidence of an impending stabilizing trend at the lowest temperature ratio investigated.

Future Plans

Plans have been made to investigate lower temperature ratios at Mach number 8 under an ABRES contract during the coming year. In anticipation of these tests, two steps have been taken to correct the problem of excessive model luminosity. First, the range model has been redesigned to reduce the

amount of model luminosity; and second, the photographic stations within the heated section of the range have been redesigned so that they are less sensitive to model luminosity. With the modified range model and the new focused shadowgraph optical system, it is anticipated that it will be possible to reduce the temperature ratio to approximately 0.025. Data in this area will be very useful in further describing the complicated behavior patterns of the boundary layer at low temperature ratios.

Before the heater is reinstalled within the range, a number of preliminary launchings will be made with the modified range model to evaluate its performance. The models will be launched at approximately 14,200 feet per second, the velocity required to produce a Mach number of 8 at the maximum desired ambient test temperature of 800°F. The purpose of the test launchings is twofold. First, they will insure that the model is structurally sound and that it can be launched at the required velocity. Second, various metals can be tested for the external surfaces to obtain the least practical amount of model luminosity at the desired test conditions. Also, the photographic stations in the heated section of the range will be changed from the divergent source shadowgraphs to the focused shadowgraphs which are much less sensitive to model luminosity.

References

(3.1) Lees, L., "The Stability of the Laminar Boundary Layer in a Compressible Fluid," NACA Report No. 876, 1947.

(3.2) Jack, J. R., Wisniewski, R. J., and Diaconis, N. S., "Effects of Extreme Surface Cooling on Boundary Layer Transition," NACA TN 4094, Oct 1957.

(3.3) Diaconis, N. S., Wisniewski, R. J., and Jack, J. R., "Heat Transfer and Boundary Layer Transition on Two Blunt Bodies at Mach Number 3.12," NACA TN 4099, Oct 1957.

(3.4) Cooper, M., Mayo, E. E., and Julius, J. E., "The Influence of Low Wall Temperature on Boundary Layer Transition and Local Heat Transfer on 2-Inch Diameter Hemispheres at a Mach Number of 4.95 and a Reynolds Number Per Foot of 7.32×10^6," NASA TN D-391, Jul 1960.

(3.5) Reshotko, E., "Transition Reversal and Tollmien-Schlichting Instability," Journal of the Physics of Fluids, Vol. 6, No. 3, 1963 pp. 335-342.

(3.6) Lyons, W. C., Jr., and Sheetz, N. W., Jr., "Free-Flight Experimental Investigations of the Effect of Boundary Layer Cooling on Transition," U. S. Naval Ordnance Laboratory NOLTR 61-83, Sep 1961.

(3.7) Sheetz, N. W., Jr., "Free-Flight Boundary Layer Transition Investigations at Hypersonic Speeds," AIAA Preprint No. 65-127, 1965.

(3.8) Staff of the Computing Section, Center of Analysis (under direction of Zdenek Kopal), "Tables of Supersonic Flow Around Yawing Cones," M.I.T. Technical Report No. 3, 1947.

(3.9) Ames Research Staff, "Equations, Tables, and Charts for Compressible Flow," NACA Report No. 1135, 1953.

(3.10) van Driest, E. R., "Investigation of the Laminar Boundary Layer in Compressible Fluids Using the Crocco Method," Report No. AL-1183, North American Aviation, Inc., Jan 1951.

(3.11) Wisniewski, R. J., and Jack, J. R., "Recent Studies on the Effect of Cooling on Boundary Layer Transition at Mach 4," Journal of the Aerospace Sciences, Vol. 28, No. 3, Mar 1961 p. 250.

TABLE 3.1 TEST CONDITIONS AND TRANSITION VALUES FOR MACH NUMBER 5 TESTS

Round	M_∞	T_∞ (^oR)	P_∞ (mm Hg)	S_{tr} (in.)	$\frac{R_e \times 10^{-6}}{L}$ (in.$^{-1}$)	$R_{tr} \times 10^{-6}$	R_θ	$\frac{T_w}{T_r}$
5036	4.53	829	764	3.12	1.75	5.46	865	.152
5037	4.52	819	749	2.95	1.78	5.25	849	.153
5039	5.15	535	455	4.40	2.10	9.23	1092	.182
5040	5.11	536	441	4.02	2.02	8.11	1022	.186
5041	4.85	770	737	2.94	1.79	5.25	843	.142
5042	4.85	787	741	2.26	1.95	4.40	772	.134
5043	4.86	535	600	3.51	2.62	9.20	1095	.202
5049	5.50	955	932	2.66	2.88	7.67	991	.091
5050	5.17	1,013	1,224	2.12	2.53	5.36	848	.098
5051	4.85	880	899	>2.88	2.11	>6.07		.131
5467	4.89	970	1,051	2.38	2.09	4.98	821	.107
5468	5.03	1,090	1,183	1.92	2.30	4.42	771	.092
5469	4.44	860	893	2.55	1.93	4.91	826	.142
5470	4.96	870	896	2.05	2.29	4.69	802	.118
5499	5.20	1,160	1,313	>2.88	2.41	>6.94		.082

TABLE 3.2 TEST CONDITIONS AND TRANSITION VALUES FOR MACH NUMBER 8 TESTS

Round	M_∞	T_∞ (°R)	P_∞ (mm Hg)	S_{tr} (in.)	$\frac{R_e}{L} \times 10^{-6}$ (in.$^{-1}$)	$R_{tr} \times 10^{-6}$	R_ψ	$\frac{T_w}{T_r}$
5462	7.66	535	503	2.50	3.73	9.32	1056	.091
5474	8.29	533	538	2.53	4.57	11.56	1161	.077
5475	7.63	660	648	1.98	3.68	7.29	935	.072
5476	7.93	860	883	1.56	3.73	5.82	828	.054
5479	8.20	860	886	1.06	4.33	4.59	749	.050
5480	8.17	850	380	>2.86	1.95	>5.59		.050

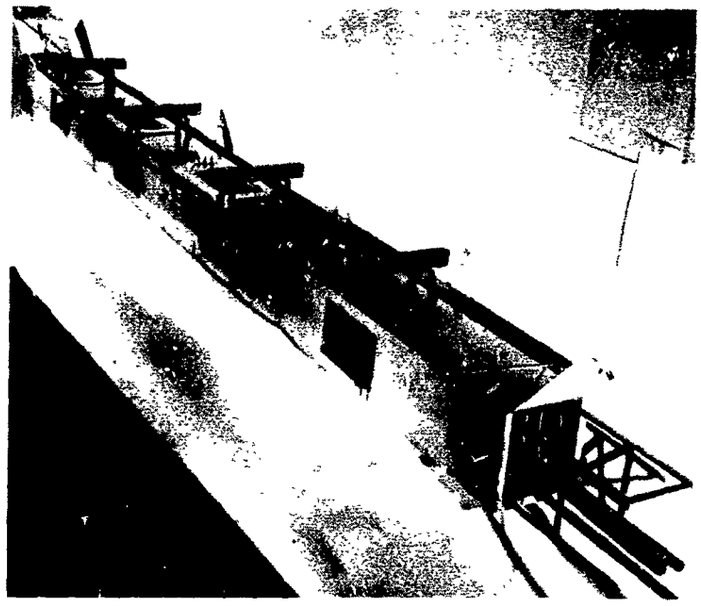

FIG.3.1 RANGE HEATER

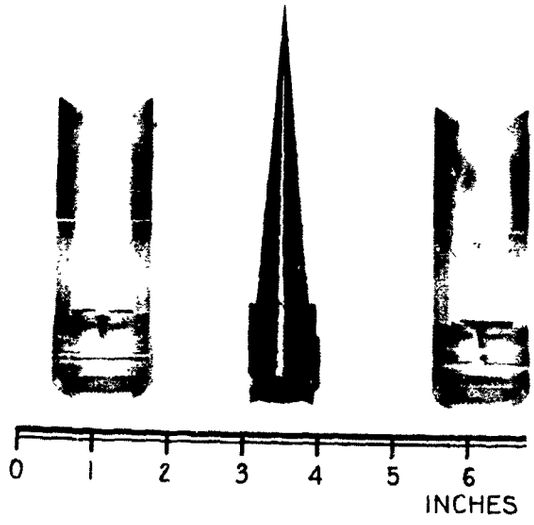

FIG 3.2 TYPICAL MODEL AND SABOT COMBINATION USED IN HEAT TRANSFER TESTS

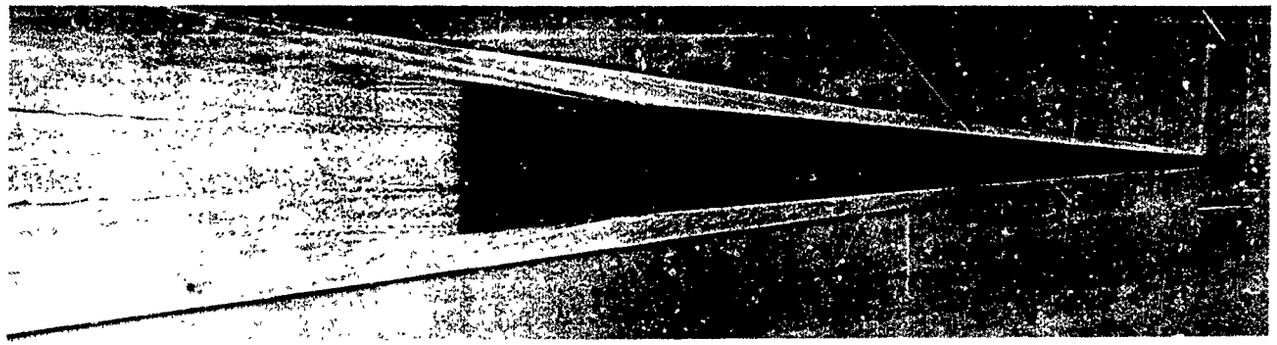

FIG. 3.3 SHADOWGRAPH OF MODEL AT LOW ANGLE OF ATTACK WITH TRANSITION OCCURRING SYMMETRICALLY

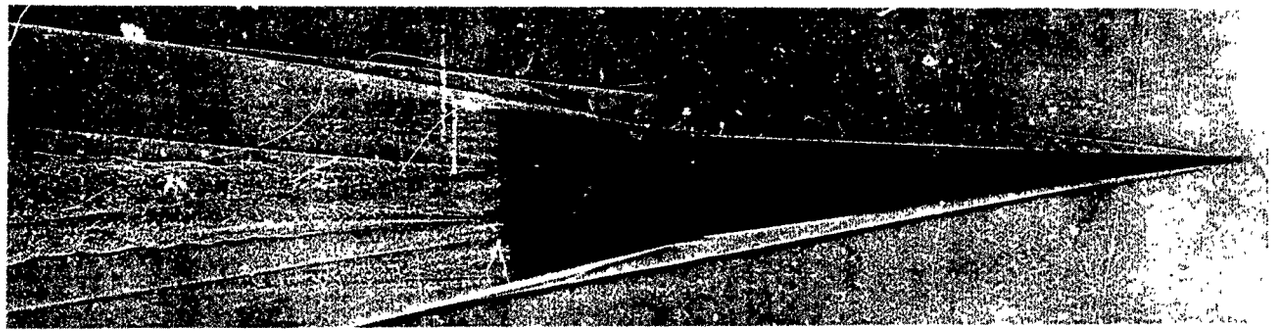

FIG. 3.4 SHADOWGRAPH OF YAWING MODEL WITH TRANSITION OCCURRING UNSYMMETRICALLY

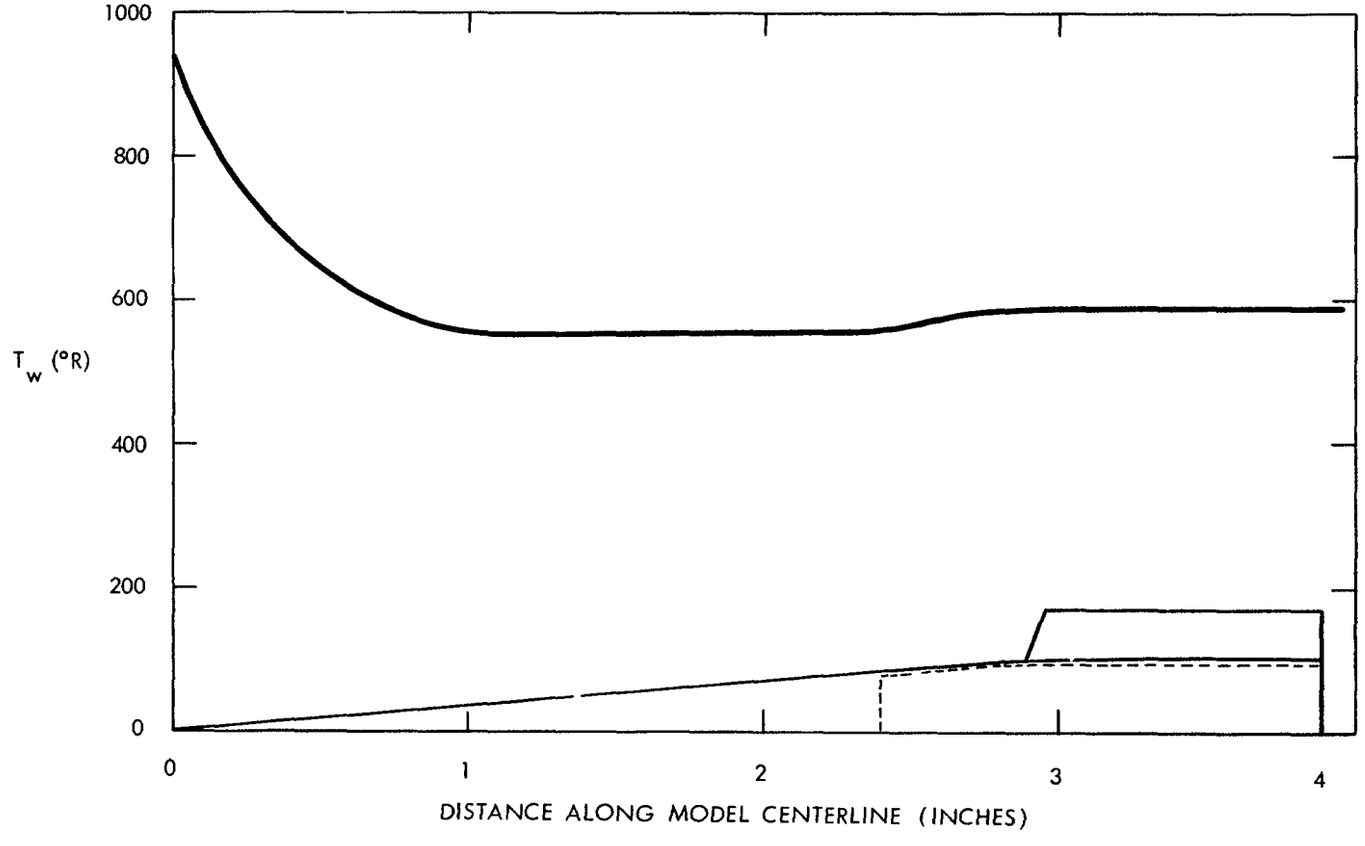

FIG. 3.5 SURFACE TEMPERATURE DISTRIBUTION AT THE END OF THE HEATED SECTION OF THE RANGE

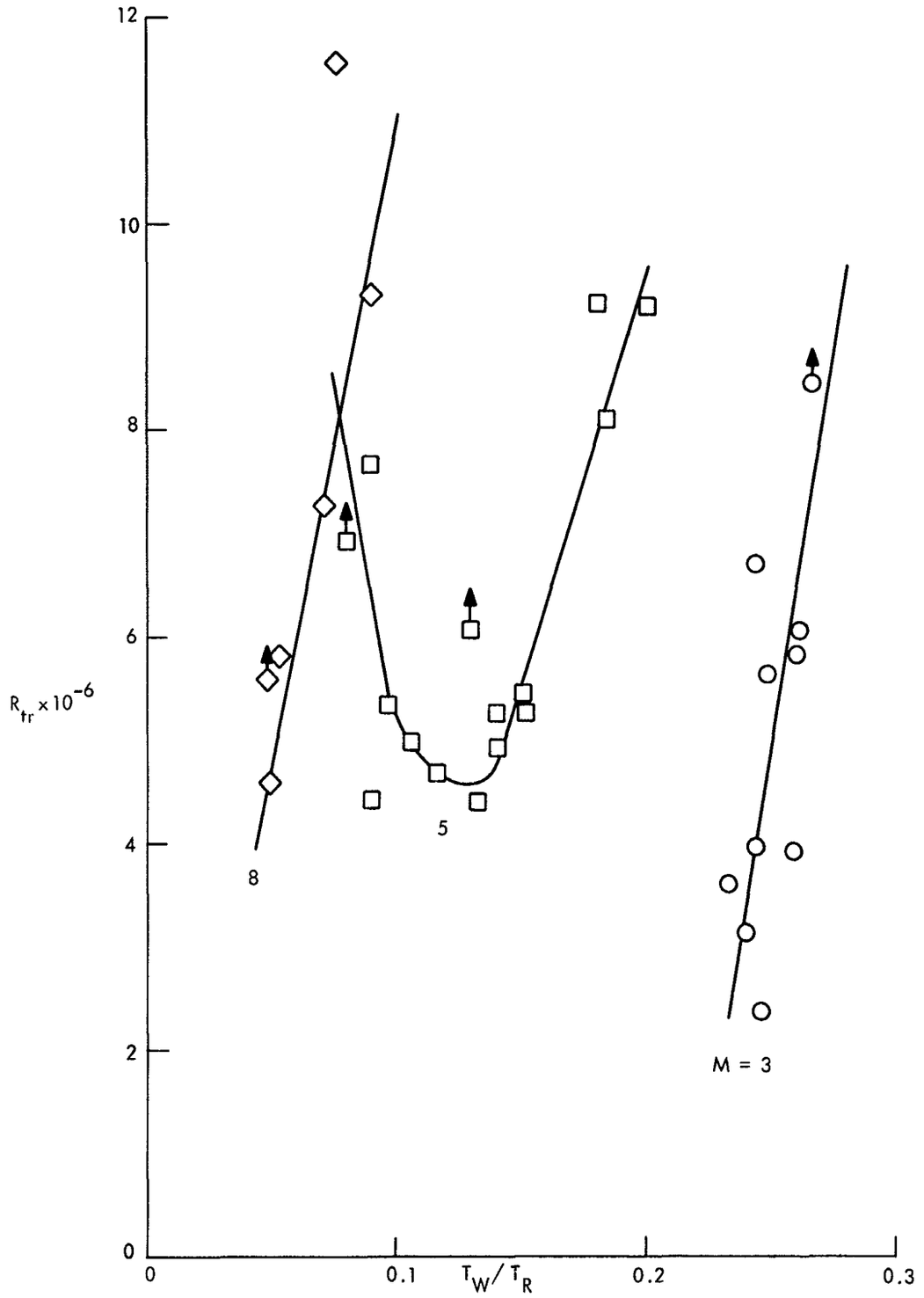

FIG. 3.6 EFFECT OF TEMPERATURE RATIO ON LOCAL TRANSITION REYNOLDS NUMBER

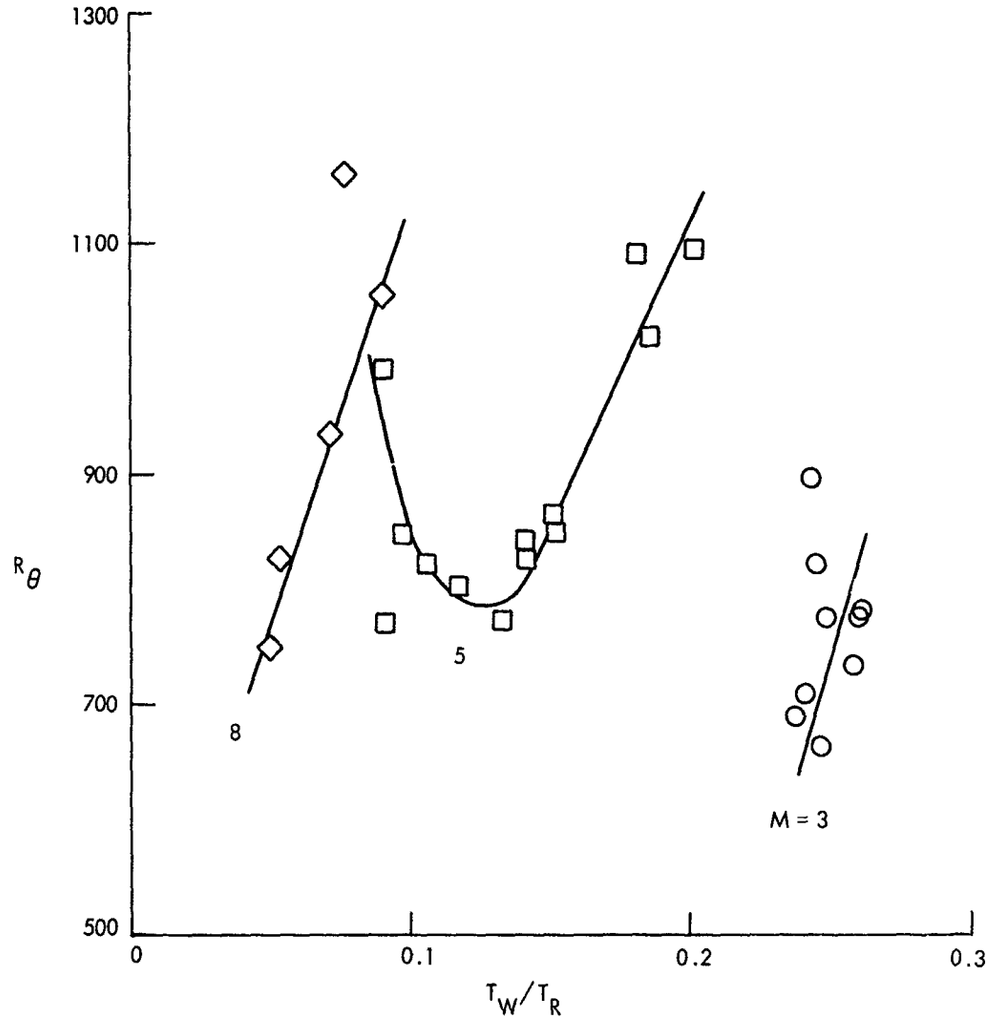

FIG. 3.7 EFFECT OF TEMPERATURE RATIO ON R_θ

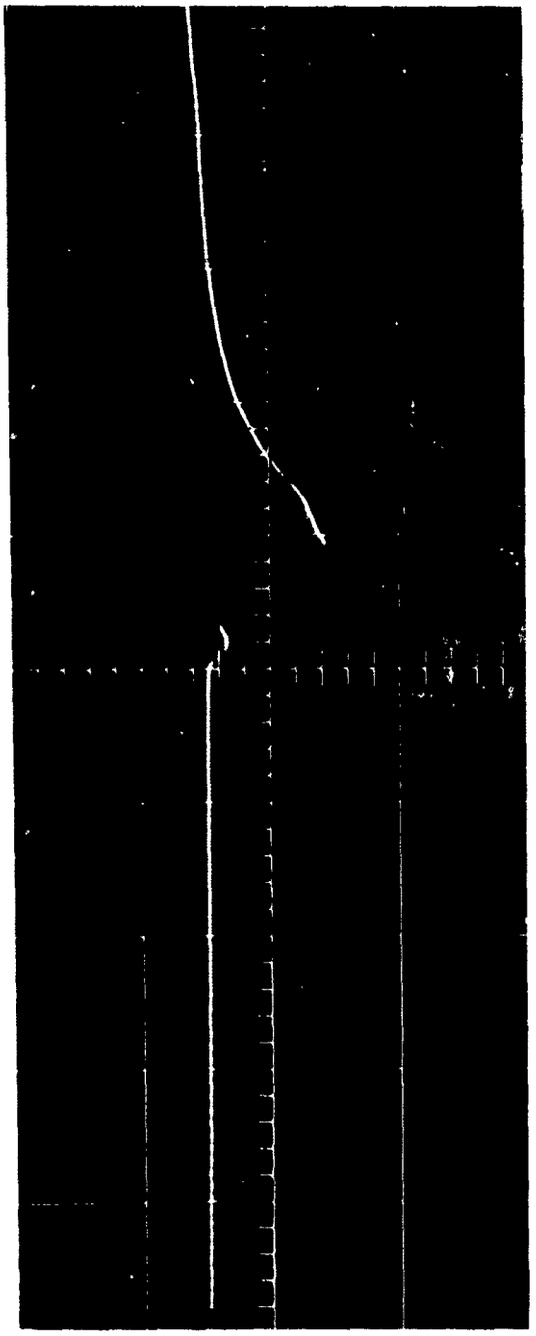

FIG. 3.8 VARIATION IN LIGHT INTENSITY AS MODEL PASSES DATA STATION

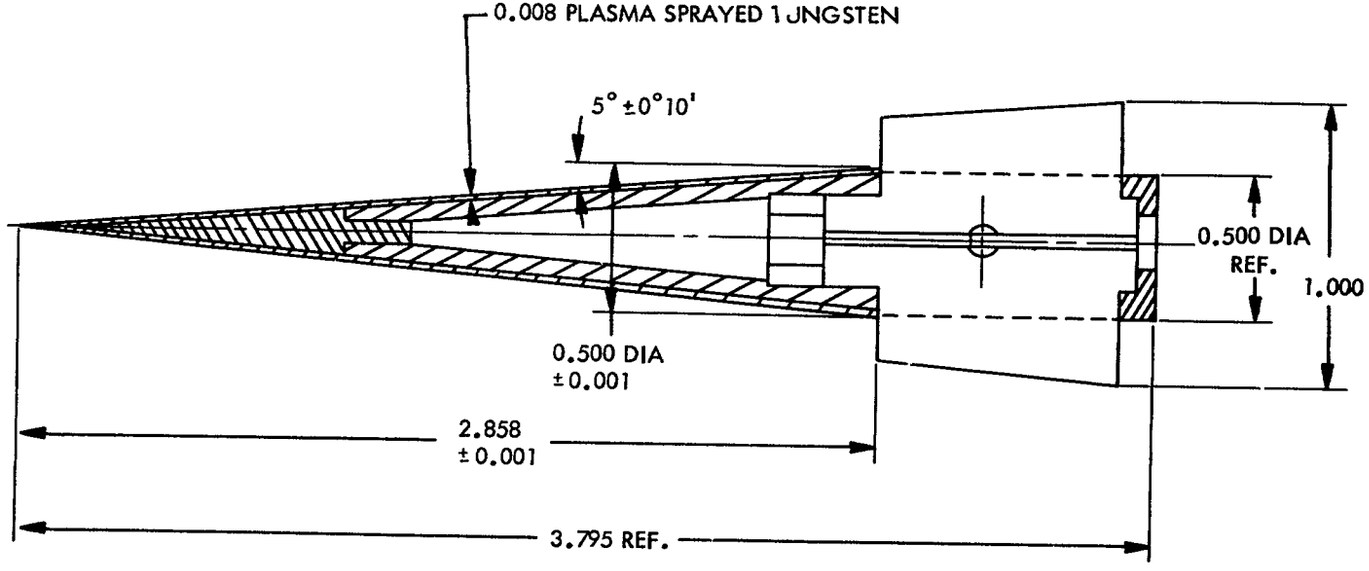

FIG. 3.9 MODIFIED TRANSITION MODEL

TASK 4.0

BODY SCALE EFFECTS ON THE AERODYNAMIC CHARACTERISTICS OF WAKES (INCLUDING SOME RESULTS ON TURBULENT EDGE ROUGHNESS)

Preliminary Comments

Results on the effects of body scale are not as extensive as originally expected due to the difficulty encountered in firing very small models at low angles of yaw.

Some results concerning the statistical analysis of the turbulence wake edge have been included, however, beyond those anticipated at the beginning of this program.

Task 4.0 has therefore been divided for discussion purposes into subtasks 4.0A and 4.0B, and these divisions will be treated in sequence.

TASK 4.0A

BODY SCALE EFFECTS

Introduction

One wake characteristic of great importance is the transition from laminar to turbulent flow. Experimental information on this subject has been obtained in several laboratories (references (4.1A) through (4.4A)). The effects of Mach number, Reynolds number and body geometry on wake transition have been investigated. More information is needed, however, through a wider range of these parameters. It is also important to determine the effect, if any, of the body scale on wake transition. Earlier results (reference (4.2A)) have shown that in a certain region of body Reynolds numbers, wake transition Reynolds number is constant and relatively independent of body Reynolds number for a fixed value of Mach number. These results were obtained from data on small cones of nearly the same size.

The present results are reported for 9-degree half-angle cones with 0.05 nose to base radius ratios. Cone size varied from 0.25 to 1.4 inches base diameter. The Mach number was 10.3, and the Reynolds numbers varied from 2×10^4 to 1.3×10^6.

Description of Experiment

Launchings were made of 9-degree half-angle cones with 0.05 base to nose radius ratio and base diameters of 0.10, 0.25, 0.30, 0.60 and 1.40 inches.

Several attempts to launch the 0.10 inch base diameter cones failed to produce a successful launch. The launching of this size cone consistently at low values of yaw angle will require a developmental program.

Cones were constructed of titanium with hollow bases to achieve satisfactory location of the center of gravity. Control launchings at NOL with closed bases have shown no observable effect due to an open base.

The characteristics of the facilities used in this program are listed in Tables 1.2 and 1.3, and the experimental technique is covered by the description in Task 5.0.

Discussion of Results

Figure 4.1 is a shadowgraph of one of the firings in the 1000-foot Hyperballistics Range. The model is of 1.4 inch base diameter. The quality and detail of this photograph is considerably less than those obtained with the smaller models in the Pressurized Ballistics Range.

Evaluation of the results of this task should be carried out in conjunction with the results of Task 5.0. In that section it will be shown that Mach number and wall to stagnation enthalpy ratio must be considered when interpreting wake transition results. The transition data presented in this task (4.0) have been corrected for Mach number effects using the results of Task 5.0.

The wake transition results for Mach number 10.3 and two values of wall to stagnation enthalpy ratio are presented in figure 4.2. Wake transition Reynolds numbers R_{x_1} and R_{x_2} are plotted versus body Reynolds number R_d. The definition and meaning of R_{x_1} and R_{x_2} are discussed at greater length in Task 5.0. Briefly, R_{x_1} represents the initial departure from laminar flow and R_{x_2} represents established random turbulence. The region to the right of R_d of approximately 10^6 represents transition in the near base region or on the body. The region covered by the range of body Reynolds numbers from 3×10^5 to 1.2×10^6 represents the major portion of the present investigation. In this region no significant effect of body scale on transition Reynolds number can be seen.

In the region to the left of an R_d value of 3×10^5 only fragmentary information is available. Two important effects appear to be present, however, as indicated by the arrows on figure 4.2. First, the wake transition Reynolds numbers (and particularly R_{x_1}) appear to be strongly influenced by the yaw angle and possibly the yaw rate of the vehicle. Second, at low or zero yaw the indications are that wake transition Reynolds numbers may increase markedly with decreasing values of R_d.

Some wake transition results obtained at NOL in other investigations are presented in figure 4.3. These results are for the same body configuration at Mach numbers of approximately 15. The results have been corrected in a manner similar to those of figure 4.2. The body Reynolds number range is similar to that of the other data and similarly no effect of body Reynolds number on wake transition Reynolds number is noted.

Future Work

There is a strong need for developing dependable launching techniques required for small bodies at low pressures and yaw angles. The study of wake transition and other wake and flow characteristics at very low values of pressure and high velocities is severely compromised by present launching and firing limitations.

References

(4.1A) Slattery, R. E., and Clay, W. G., "The Turbulent Wake of Hypersonic Bodies," ARS Seventeenth Annual Meeting and Space Flight Exposition, Nov 1962.

(4.2A) Lyons, W. C., Jr., Brady, J. J., and Levensteins, Z. J., "Hypersonic Drag, Stability, and Wake Data for Cones and Spheres," AIAA Journal, Vol. 2, 1964 pp. 1948-1956.

(4.3A) Pallone, A., Erdos, J., and Eckerman, J., "Hypersonic Laminar Wakes and Transition Studies," AIAA Journal, Vol. 2, 1964 pp. 855-863.

(4.4A) Wilson, L. N., "Body Shape Effects on Axisymmetric Wakes," GM Defense Research Laboratories, TR 64-02K, Oct 1964.

TASK 4.03

STATISTICAL ANALYSIS OF THE TURBULENT WAKE EDGE BEHIND HYPERSONIC CONES

Introduction

Knowledge of the behavior of the turbulent wake edge is of importance for two reasons. First, knowledge of the edge roughness characteristics may be needed for interpretation of radar data from over-dense plasma conditions. Second, the surface roughness characteristics may provide information on the parameters of the inner wake flow.

Some results on statistical properties of the edge of the turbulent wake have been obtained. They are used to describe the roughness of the wake edge and how it varies with distance behind the body. The quantities measured include the standard deviation of the intermittent zone of the wake, the intermittency distribution, the autocorrelation function, the correlation microscale, and the integral scale.

Corrsin and Kistler (reference (4.1B)) were the first to study the intermittent zone between turbulent and non-turbulent fluid and relate the characteristics of this region to those of the inner turbulence. Three low speed, incompressible turbulent shear flows were considered: rough-wall boundary layer, plane wake behind a cylinder, and round jet. Recently Shapher (reference (4.2B)) has applied the relations established by Corrsin and Kistler to high speed sphere and cone wakes.

It is the purpose of the present investigation to study the roughness of the turbulent edge as it appears on shadowgraph photographs behind a hypersonic cone. From such a two dimensional projection, it is difficult or impossible to describe how the turbulent eddies were positioned in the wake when the picture was taken. The actual wake is a three-dimensional structure with turbulent eddies in front and behind other eddies. All that can be seen on a

shadowgraph is their two dimensional projection - an outline of their peaks. This outline, called the edge, has been analyzed to determine its roughness and how it grows with distance behind the body.

Experimental Procedure

A 9-degree half angle, .25-inch base diameter cone was fired in the NOL Pressurized Ballistics Range with shadowgraph coverage of its wake up to 900 body diameters behind the body. It was fired in air at Mach number 10.6 and at a pressure of 260 mm Hg. The shadowgraph pictures obtained are 17 inches long but the image on these plates is magnified because of the divergence of the light from the spark source. The magnification factor was obtained from the position of the wake between the spark and the photographic plate. In this case, tne image on the plate was enlarged by a factor of 1.28. Six plates from this shot were obtained at 23.5, 144, 318, 702, 798, and 894 diameters behind the body. These numbers represent the distance from the base of the cone to the center of the section of the wake.

The first objective, after the plates were obtained, was to describe the edge of the wake numerically. A reference line was drawn near the center of the wake and generally paralleled to it. Distances, y_n, from this line to the edge of the wake were measured at intervals $\Delta x = 0.779$ mm along its length. This was done on the

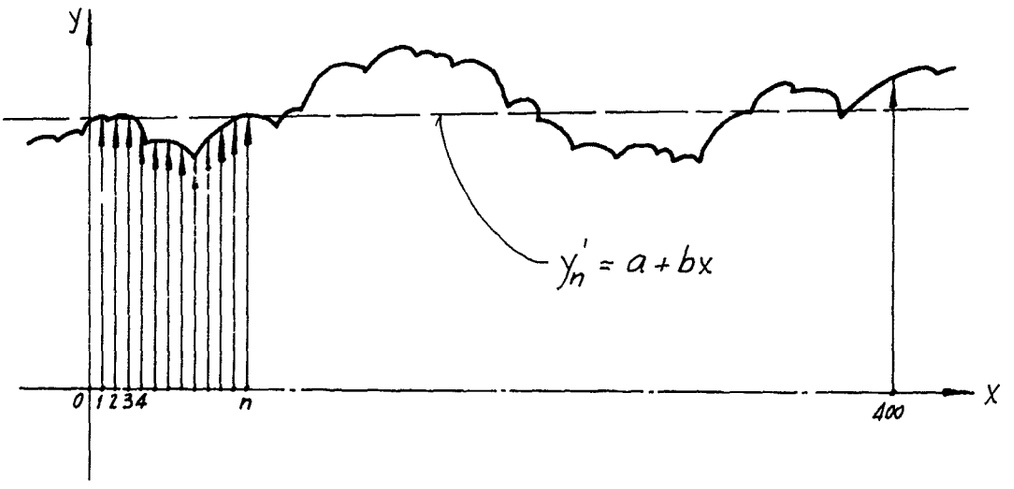

Contact Telereader made by the Telecomputing Corporation and the coordinates of the edge punched out on IBM data cards directly. Four hundred such measurements were made on each plate, wherever possible. On the two photographic plates of the wake near the body, only 250 measurements could be read. Only one side of the wake was described. The other side, probably due to angle of attack, was slightly fogged. All computations were done on the IBM 7090 digital computer.

A straight line was fitted through the measured points, y_n, by the method of least squares,

$$y_n' = a + bx$$

Then deviations, ϵ_n, about this line were generated by subtracting the appropriate distances, such that,

$$\epsilon_n = y_n - y_n' .$$

The condition that the mean of the deviations about the newly defined line is zero is satisfied automatically, $\Sigma \epsilon_n = 0$. All of the statistical properties were computed from the ϵ_n-ensemble. For convenience in describing the statistical operations, the dispersion of these deviations will be known as g(x).

Analysis and Discussion

As a measure of the roughness of the turbulent wake edge or the width of the intermittent zone, the standard deviation, σ, about the mean was computed,

$$\sigma = \left[\int_0^{\ell} g^2(x)\, dx \right]^{1/2},$$

where l is the length of the sample. After it was reduced by the proper magnification factor and divided by the body diameter, d, it was plotted against the downstream distance x/d in figure 4.7. It represents the roughness measurement in a direction perpendicular to the flight path of the cone, since the interval between the readings does not enter into the above computation. It is seen that near the body the normalized standard deviation has a value of about .065 and exhibits a relatively slow growth rate. The roughness increases sharply past 150 body diameters and at 1,000 diameters, $\sigma/d = .27$.

Intermittency factor was defined by Townsend (reference (4.3B)) as the fraction of the time a fixed probe spends in a turbulent fluid. The same definition can be applied to the present case where the time in the above definition is replaced by distance. Intermittency factor for a given distance, y, away from the least squares line was obtained by adding all of the turbulent sections and dividing by the sample length, l. This gives the probability that at a given y the fluid is turbulent. The procedure was repeated throughout the intermittent zone and the results plotted in figure 4.4. It is seen that the width of the intermittent zone is increasing with distance behind the body. When the y coordinate is divided by the standard deviation, σ, the distributions of intermittency show good similarity at all of the sections of the wake considered. Furthermore, when they are compared with the theoretical Gaussian distribution, it is found, in figure 4.5, that they satisfy this distribution. This turns out to be a very important result and will find its application in the computation of the correlation microscale, λ.

The autocovariance function, $A(\xi)$ is defined (1) as

$$A(\xi) = \int_0^{\ell} g(x)g(x+\xi)\,dx.$$

The autocorrelation function, $R(\xi)$, is the above relation normalized by itself when the displacement, ξ, is zero:

$$R(\xi) = \frac{A(\xi)}{A(0)} = \frac{\int_0^\ell g(x)g(x+\xi)dx}{\int_0^\ell g^2(x)dx} = \frac{1}{\sigma^2}\int_0^\ell g(x)g(x+\xi)dx .$$

This function was calculated for the sections of wake read and the results are presented in figure 4.6. Since the autocorrelation function was generated by displacements in the x-direction and normalized so that it always has a value of one at $\xi = 0$, it can only provide information of the scales of roughness in the direction of the flight of the cone. Two such scales have been obtained: the integral scale, L, and the microscale, λ.

The integral scale, L, is defined by the area under the autocorrelation curve (reference (4.5B))

$$L = \int_0^\infty R(\xi)d\xi .$$

In practice, however, at large values of ξ the autocorrelation function $R(\xi)$ does not approach zero, but oscillates about the $R(\xi) = 0$ line. Therefore, the integral cannot be evaluated. This problem is introduced by an insufficient number of independent samples. It has been noticed that at small values of ξ, the autocorrelation function closely behaves as an exponential function, $e^{-\xi}$. Therefore, Slattery and Clay (reference (4.6B)) have defined their correlation scale L as that value of ξ where $R(\xi)$ drops to 1/e of its

original value. This definition of the integral scale L has been used as an approximation in the present study.

The values of integral scale were measured from the curves in figure 4.6 and plotted versus distance behind the cone in figure 4.7. It is seen that the roughness growth as exhibited by the integral scale is very similar to that of the standard deviation, differing only in the numerical value. Up to 150 diameters it has a value of about .2 and increases past tnat point to about .7 at 1,000 diameters.

The correlation microscale is defined bv the osculating parabola to the autocorrelation function at $\xi = 0$ (reference (4.5B)). Since the autocorrelation function near $\xi/d = 0$ is not well defined in the present case, it does not seem feasible to obtain microscale from this definition. But the nearly Gaussian character of the intermittency distribution permits the application of the result derived by Corrsin and Kistler (reference (4.1B)) which related the zero occurrences of g(x) with correlation microscale. The microscale is approximately given by

$$\lambda = \frac{\sqrt{2}}{\pi} \frac{1}{N_o},$$

where N_o is the number of times g(x) takes a value of zero per unit length of record. This quantity was computed for the six sections of the wake edge and plotted against x/d in figure 4.7. It is seen that the microscale has nearly the same value as the integral scale and grows in the same way. In fact, all three of the measured scales have almost identical growth characteristics. This means that the turbulent eddies that describe the edge of the wake do not have a preferred direction of growth, but expand at the same rate in both directions.

Conclusions

The edge of the turbulent wake was described numerically and three scales of edge roughness calculated. The standard deviation about mean gives a measure of roughness in a direction normal to the flight path. Correlation microscale and integral scale are measures of roughness in the flight direction. Scales show similar growth characteristics.

References

(4.1B) Corrsin, S., and Kistler, A. L., "Free-Stream Boundaries of Turbulent Flows," NACA Report 1244, 1955.

(4.2B) Schapker, R. L., "Turbulence Front Statistics of Wakes from Bodies in High-Speed Flight," AVCO-Everett Research Laboratory, Research Report 217, Jun 1965.

(4.3B) Townsend, A. A., "Momentum and Energy Diffusion in the Turbulent Wake of a Cylinder," Proceedings of the Royal Society of London, Vol. 197, May 1949, p 130.

(4.4B) Blackman, R. B., and Tukey, J. W., The Measurement of Power Spectra, Dover Publications, 1958.

(4.5B) Lumley, J. L., and Panofsky, H. A., The Structure of Atmospheric Turbulence, John Wiley & Sons, 1964, p 15.

(4.6B) Slattery, R. E., and Clay, W. C., "The Turbulent Wake of Hypersonic Bodies," ARS Seventeenth Annual Meeting and Space Flight Exposition, Nov 1962.

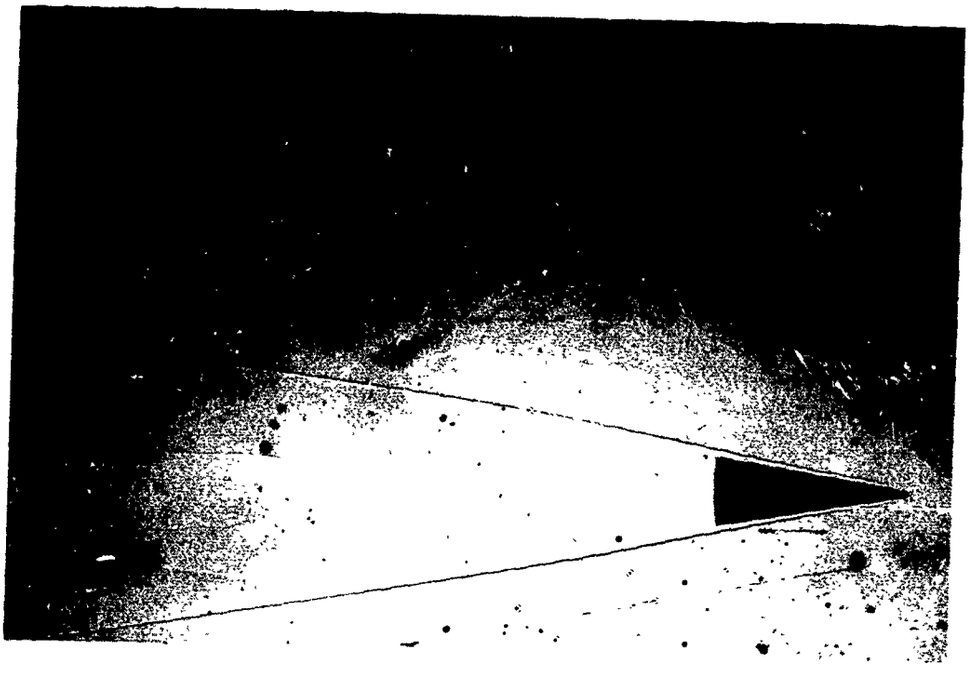

FIG. 4.1 SHADOWGRAPH OF CONE FOR BODY SCALE EFFECTS INVESTIGATION
$M_\infty = 11.1$ $R_{\infty_d} = 9.28 \times 10^5$

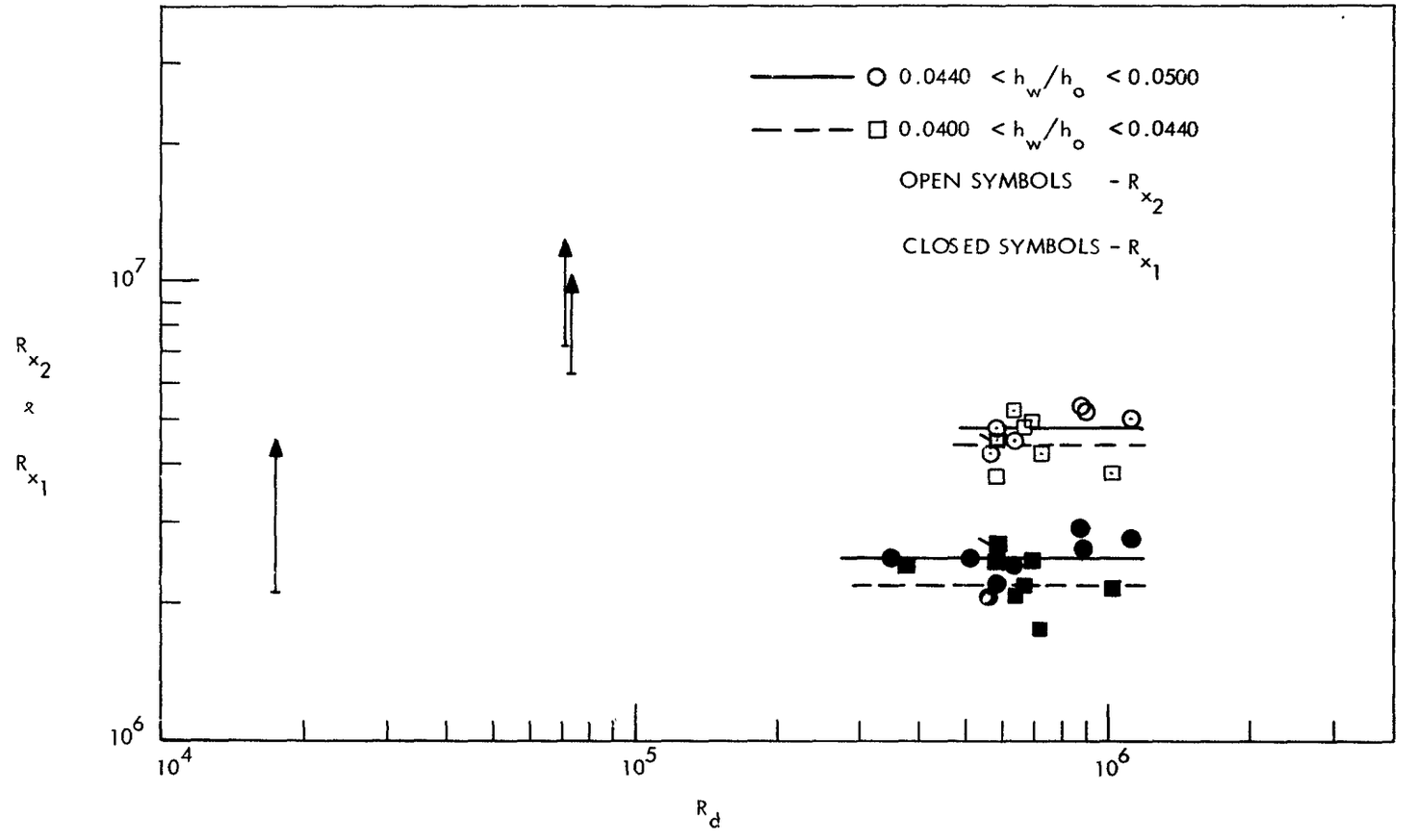

FIG. 4.2 THE EFFECT OF BODY REYNOLDS NUMBER ON WAKE TRANSITION REYNOLDS NUMBER AT MACH NUMBER 10.3

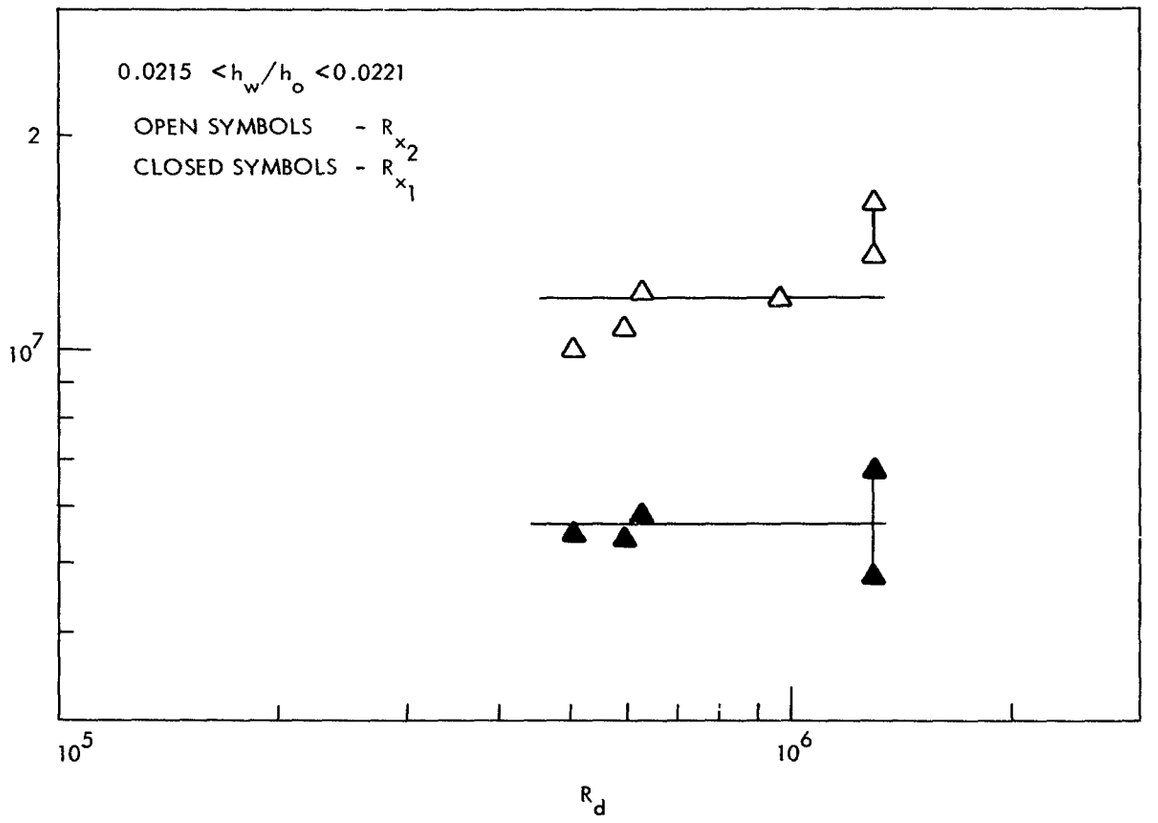

FIG. 4.3 THE EFFECT OF BODY REYNOLDS NUMBER ON WAKE TRANSITION REYNOLDS NUMBER AT MACH NUMBER 15.0

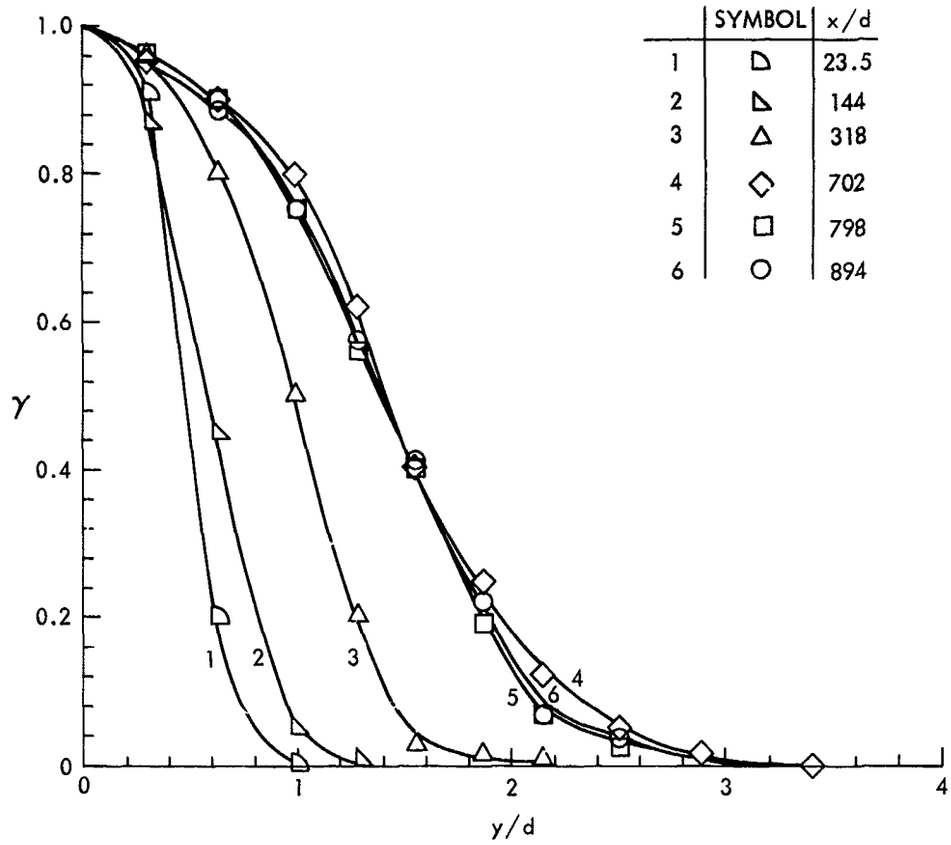

FIG. 4.4 INTERMITTENCY DISTRIBUTIONS FOR TURBULENT WAKE EDGE AT SEVERAL STATIONS BEHIND THE BODY.

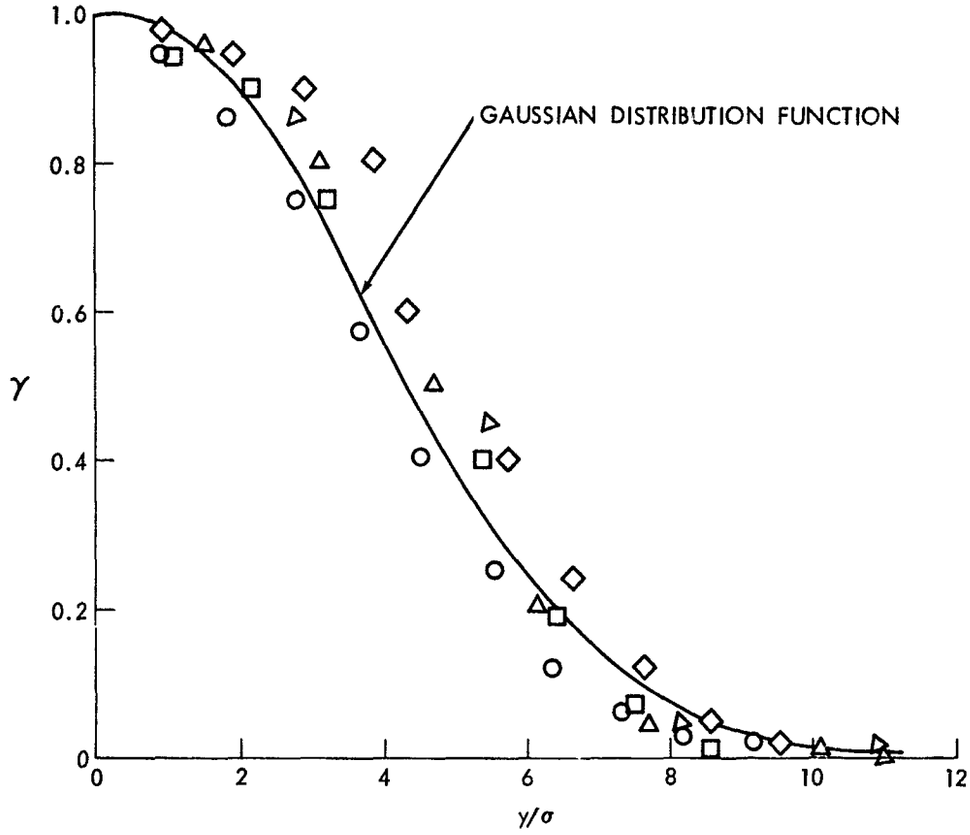

FIG. 4.5 INTERMITTENCY DISTRIBUTION FOR THE TURBULENT WAKE EDGE COMPARED TO GAUSSIAN DISTRIBUTION FUNCTION

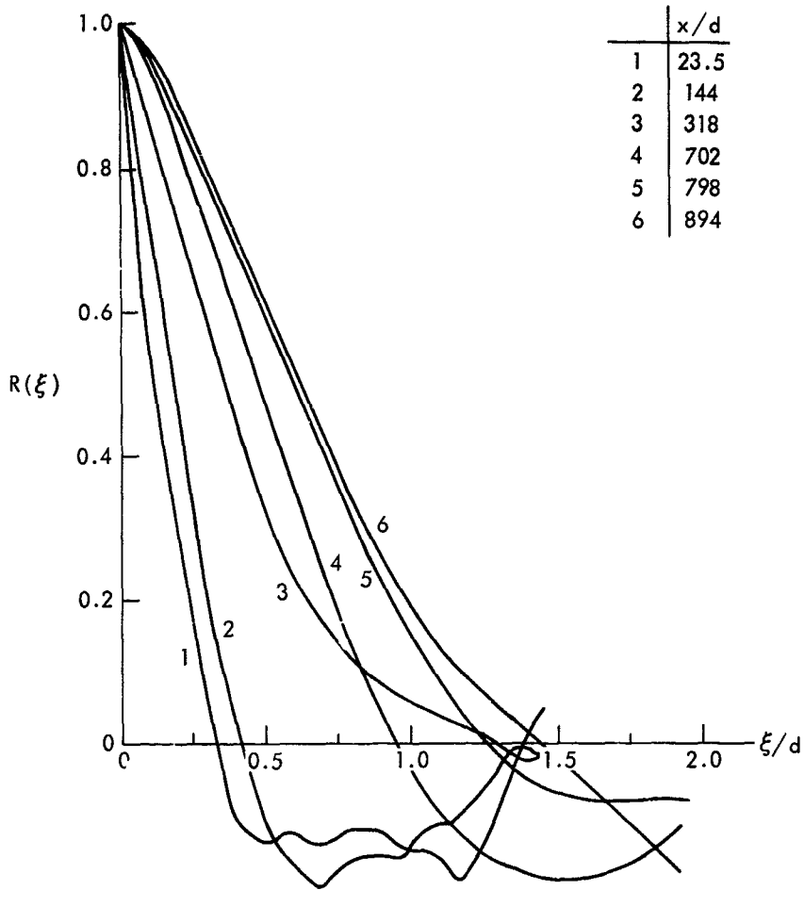

FIG. 4.6 AUTOCORRELATION FUNCTIONS OF THE WAKE EDGE AT SEVERAL STATIONS BEHIND THE BODY.

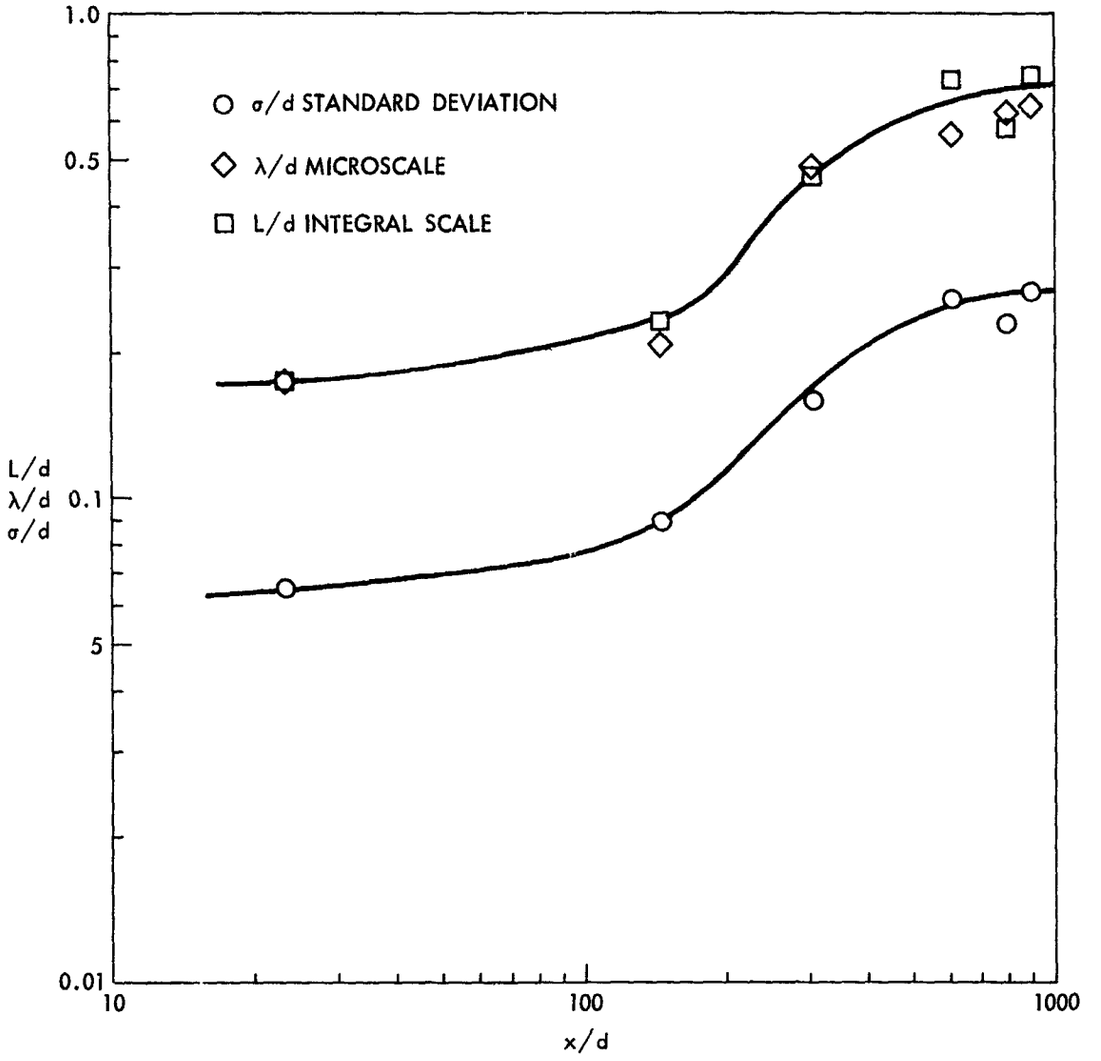

FIG. 4.7 STATISTICAL PARAMETERS OF THE EDGE OF THE TURBULENT WAKE AS A FUNCTION OF DISTANCE BEHIND THE CONE

TASK 5.0

THE EFFECT OF HEAT TRANSFER ON THE AERODYNAMIC CHARACTERISTICS OF WAKES

Introduction

During the last few years much effort has gone into both theoretical and experimental study of wake flow. A knowledge of the characteristics of the flow in the wake behind hypervelocity objects is of great practical importance because these characteristics can be related to the objects themselves. For a complete aerodynamic understanding, the effects of Mach number, Reynolds number, and surface heat transfer on the wake flow must be known. One important characteristic of the viscous wake flow is its stability and the eventual transition from laminar to turbulent motion. Some theoretical (references (5.1) and (5.2)) and a great deal of experimental work (references (5.3), (5.4), (5.5), and (5.6)) has been done to gain insight into the mechanism of these phenomena. The Mach number effects and, in a certain range, the Reynolds number effects on the wake transition characteristics are reasonably well known (references (5.3) and (5.4)). There was no information available, however, on the effects of surface heat transfer or wall to stagnation enthalpy ratio. At hypervelocity flight conditions in the atmosphere the stagnation enthalpy of the flow is extremely high and the wall to stagnation enthalpy ratio is very small. A simulation of this flow parameter can be achieved in a ballistics range. However, to investigate the effect of the wall to stagnation enthalpy ratio on the wake flow characteristic, this parameter must vary over a reasonable range for constant Mach number and Reynolds number conditions. In this program the effects on the laminar to turbulent wake flow transition and base flow geometry were investigated in the wall to stagnation enthalpy ratio range between 0.03 and 0.08. In order to vary the wall to stagnation enthalpy ratio at constant Mach number, there must be a capability to adjust the ambient pressure, temperature, and model velocity in the ballistics range. The investigation was conducted in the NOL Pressurized Ballistics Range where such capabilities exist. The flight Mach numbers in this program

were 8.4 and 10.3, and the body Reynolds numbers were in the region where wake transition Reynolds numbers are independent of body Reynolds number.

Description of Experiment

The model configuration for this program was a 9-degree half-angle cone with a 0.05 nose to base radius ratio. The base diameter of the cones was 0.87 inch. The cones were made of titanium and had hollow bases. It has been shown in other experiments conducted in NOL ballistics ranges that the hollow model base has no measurable effect on either the base flow geometry or the laminar to turbulent flow transition. The cones were nonablating.

The firings were conducted in the Pressurized Ballistics Range. The characteristics of this facility are listed in Table 1.3 of the Task 1.0 Report. Briefly, there is a section of the range in which the ambient temperature can be adjusted between approximately 80°F and 800°F. In order to vary the stagnation enthalpy of the flow at a constant Mach number, the cones were fired at different velocities thus producing different amounts of kinetic energy in the flow. Simultaneously the ambient temperature in the heated section of the range was adjusted so that the flight Mach number was at the desired constant value. With the present capabilities of the heated range section a wall to stagnation enthalpy ratio, h_w/h_o, variation between 0.03 and 0.08 was possible for Mach number 8.4 and between 0.03 and 0.05 for Mach number 10.3. In these ratios the wall enthalpy h_w was assumed to be constant and equal to the ambient room enthalpy. Because of the short flight times, this is a good assumption except for the tip region of the cone.

A total of 21 cones were fired in this program. The experimental data were obtained from various measurements made of the base and wake flow phenomena as they appear on spark shadowgraphs. The following sketch helps to identify these measurements.

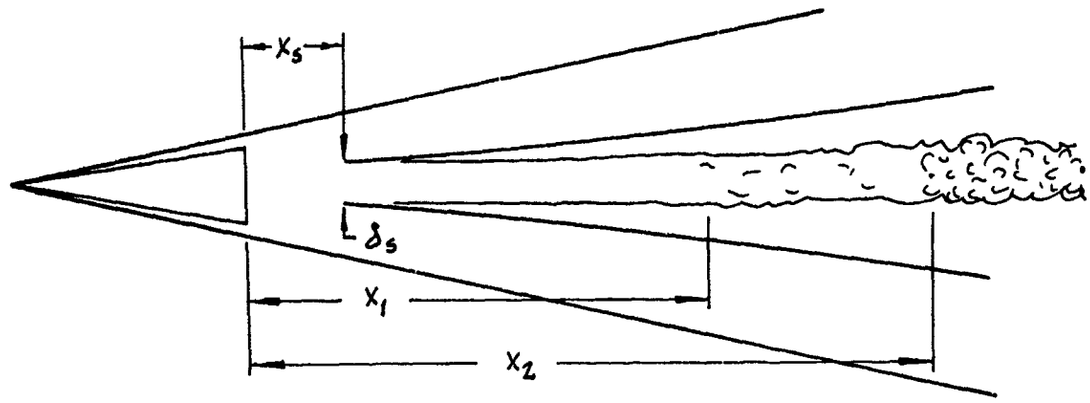

In the laminar to turbulent wake flow transition measurements the quantity x_1 is defined as the axial distance from the base of the model to the very first appearance of laminar waves in the viscous wake. The quantity x_2 is defined as the axial distance from the base of the model to the first appearance of random fully turbulent flow. Thus, the difference between x_2 and x_1 is the length of the transitional region in the viscous flow.

In a study of shadowgraph photographs of wake flow, it is rarely possible to determine a single point in the flow where the events just discussed occur. Rather, there is a small zone of uncertainty within which the character of the flow changes. This uncertainty introduces some subjectivity in the readings. Fortunately, experience shows that by studying and reading a large number of shadowgraphs, a given individual measures the phenomena quite consistently. The variations in measurements among various readers have also proven to be within reasonable limits.

The amount of laminar flow details in the base flow visible with the shadowgraph technique depends greatly on the flight Mach number. Up to about Mach number 7 there is a line discernible which extends between the expanding boundary layer at the shoulder of the model and the recompression region of the wake flow. Most likely, this line is the edge of the free-shear layer. At higher flight

Mach numbers, however, there is absolutely no indication of flow direction in the base flow. Some distance downstream of the base of the model, the wake recompression shocks become visible. It was decided to make two measurements on the shadowgraphs of the hypersonic base flow that should help to define the geometry of this flow region. The measurement x_s is the distance from the base of the model to the very first appearance of the wake recompression shocks. Hopefully, this distance indicates the location of the rear stagnation point and an average inclination of the dividing streamline. The other measurement δ_s is the distance between the wake recompression shocks at their origin.

Both the laminar to turbulent wake flow transition and the base flow geometry measurements were made on several shadowgraphs obtained from any given shot. In some cases as many as twenty readings were obtained for one shot. From a trajectory analysis of the cone a complete angle of attack history for the cone was determined. From studies of the wake flow shadowgraphs it was noted that, generally, transition in the wake behind models at an angle of attack occurred closer to the body than when the models were at zero angle of attack. Also, behind cones at an angle of attack the laminar wake appeared to consist of more than one filament-like structure. Transition from laminar to turbulent flow in one filament would occur at an appreciably different location than in another filament. All these observations led to an attempt to determine the relationship between the transition distances and the angle of attack of the cones. By knowing this relationship, one could correct all the data to a common angle of attack and thus eliminate the effects of this variable. Unfortunately, no reasonable correlation could be achieved with the data available at this time. Therefore, in computing the base and wake flow parameters for a given shot, it was decided to use only those readings that were obtained from shadowgraphs where the cone was below a certain angle of attack. For the 9-degree half-angle cones used in this investigation, an angle of attack of 2 degrees was chosen as the limiting value. An arithmetic mean was computed from the shadowgraph readings below this angle of attack. Thus, the results for the various base and wake flow phenomena, which are presented, are the averages from shadowgraph readings where the cone was at an angle of attack equal to or less than 2 degrees.

Discussion of Results

All the results presented in this report are correlated with flow parameters based on ambient conditions ahead of bow shock. This is the most convenient method and is acceptable as long as only one body configuration is considered. The major flow parameter in this investigation is the wall to stagnation enthalpy ratio. The stagnation enthalpy of the flow, h_o, is computed from the energy equation $h_o = h_1 + V^2/2$, where h_1 is the ambient static enthalpy and V is the velocity of the cone. As already mentioned, the enthalpy of the wall, h_w, is assumed to be constant and equal to the enthalpy of the air prior to firing.

The laminar to turbulent wake flow transition data are correlated in terms of wake transition Reynolds numbers R_{x_1} and R_{x_2}. In figure 5.1 the wake transition Reynolds numbers are presented as functions of the enthalpy ratio h_w/h_o. The data are grouped together according to the approximate Mach numbers at which they were obtained. The round symbols are for the approximate flight Mach number of 8.4 and the triangular symbols for 10.3. It is known from work at NOL and other laboratories (references (5.3) and (5.4)) that the wake transition Reynolds numbers are quite sensitive functions of the flight Mach number. Therefore, it was necessary to correct the wake transition Reynolds numbers of figure 5.1 for Mach number effects.

Taking the wake transition Reynolds numbers within a narrow band of wall to stagnation enthalpy ratios and plotting them as functions of the flight Mach number resulted in graphs of figures 5.2, 5.3, and 5.4. The body Reynolds numbers for the results in these figures were between approximately 2×10^5 and 1.3×10^6. Earlier work at NOL (reference (5.3)) and the results of Task 4.0 of this report show that at Mach numbers of 8 to 10 in this Reynolds number range the wake transition Reynolds numbers are independent of the body Reynolds number. As already described, all of these results are for very low angle of attack conditions, and the wall to stagnation enthalpy ratio for each separate graph is practically constant. Therefore, the correlations in figures 5.2, 5.3, and 5.4 show pure Mach number effects on the wake transition Reynolds numbers. It is important to note that in the correlations of reference (5.3) where the

effect of Mach number on wake transition Reynolds numbers was shown, the results with widely different values for the wall to stagnation enthalpy ratio were plotted together. Even when done in that way, the results showed quite significant Mach number dependency. The wake transition Reynolds numbers shown in figures 5.2, 5.3, and 5.4, however, are considerably more Mach number sensitive.

The wake transition Reynolds number-Mach number correlations just discussed were used to correct all the transition results to constant Mach numbers of 8.4 and 10.3. The corrected results are shown in figure 5.5. Although there is scatter in the Mach number 10.3 results, the trends are definite for both Mach numbers. Namely, for both Mach numbers the wake transition Reynolds numbers R_{x_1} and R_{x_2} decrease with decreasing values of the wall to stagnation enthalpy ratio h_w/h_o. A correlation of the transition distances, however, shows that they increase slightly with decreasing values of h_w/h_o.

It seems that the heat transfer conditions at the wall of the body should be felt most strongly in the wake flow that is closest to the body. The information which has been discussed here was obtained at ambient pressures which for a constant Mach number produced wake transition 3 to 4 body diameters downstream of the base. Whether the noted wall to stagnation enthalpy effects would be felt in the wake flow when the ambient pressure is low and transition has moved far downstream is not known at this time. In any case, before more conclusions are drawn, a wider variation in the wall to stagnation enthalpy ratio is necessary. To obtain this, an extension of the capability of the temperature control section in the ballistics range is necessary.

There are some wake transition results for 9-degree half-angle cones obtained in other programs conducted at NOL. These results are at Mach numbers of approximately 5, 6, and 15. In figure 5.6 this additional information is presented together with the results obtained in this program, already shown in figures 5.2, 5.3, and 5.4. Only the established curves are repeated, and the respective wall to stagnation enthalpy ratios for each are indicated. By drawing short curves through the new results parallel to the established curves of Mach numbers 8 to 13 and noting the wall to stagnation enthalpy ratios, it can be reasonably stated that

the wake transition Reynolds numbers for a fixed Mach number are monotonically increasing with increasing wall to stagnation enthalpy ratios between 0.021 and 0.115.

The correlation of figure 5.6, in effect, extends the information available from figure 5.5. It is very important to remember that this description of the behavior of the laminar to turbulent flow transition holds true only when transition takes place downstream of the wake neck.

The investigation of the effects of the wall to stagnation enthalpy ratio on base flow geometry was limited by the lack of detail that could be observed in the photographs made in the temperature controlled section.

A comparison of photographs such as the one shown in figure 5.7 with typical shadowgraphs from the temperature controlled section indicates that most of the base flow detail is not discernible in the latter. In view of these considerations, it appears that the data previously presented from this program on the effect of h_w/h_o on x_s/d are not conclusive, and data with more sensitive instrumentation are needed in order to establish these effects.

The same evaluation must be made of the effects of h_w/h_o on δ_s/d as indicated in figure 5.8. Based upon the results of the present analysis, no significant effects are obvious in the range of h_w/h_o between approximately .03 and .075. More thorough examination of optical results containing more detail may provide more and different information on this effect.

Future Work

An improved shadowgraph system presently in shakedown status in the NOL Pressurized Ballistics Range shows promise of indicating better detail on launchings at the lower values of h_w/h_o (heated range). Work with the double-pass schlieren (figure 5.7) is planned to investigate base flow detail in the unheated range. Evaluation of data to be obtained with this new instrumentation equipment may contribute much needed information on base flow geometry.

References

(5.1) Lees, L., "Hypersonic Wakes and Trails," AIAA Journal, Vol. 2, 1964 pp. 417-428.

(5.2) Gold, H., "Stability of Axisymmetric Laminar Wakes," AIAA Entry Technology Conference, Oct 1964.

(5.3) Lyons, W. C., Jr., Brady, J. J., and Levensteins, Z. J., "Hypersonic Drag, Stability, and Wake Data for Cones and Spheres," AIAA Journal, Vol. 2, 1964 pp.1948-1956.

(5.4) Pallone, A., Erdos, J., and Eckerman, J., "Hypersonic Laminar Wakes and Transition Studies," AIAA Journal, Vol. 2, 1964 pp. 855-863.

(5.5) Slattery, R. E., and Clay, W. G., "The Turbulent Wake of Hypersonic Bodies," ARS Seventeenth Annual Meeting and Space Flight Exposition, Nov 1962.

(5.6) Wilson, L. N., "Body Shape Effects on Axisymmetric Wakes," GM Defense Research Laboratories, TR 64-02K, Oct 1964.

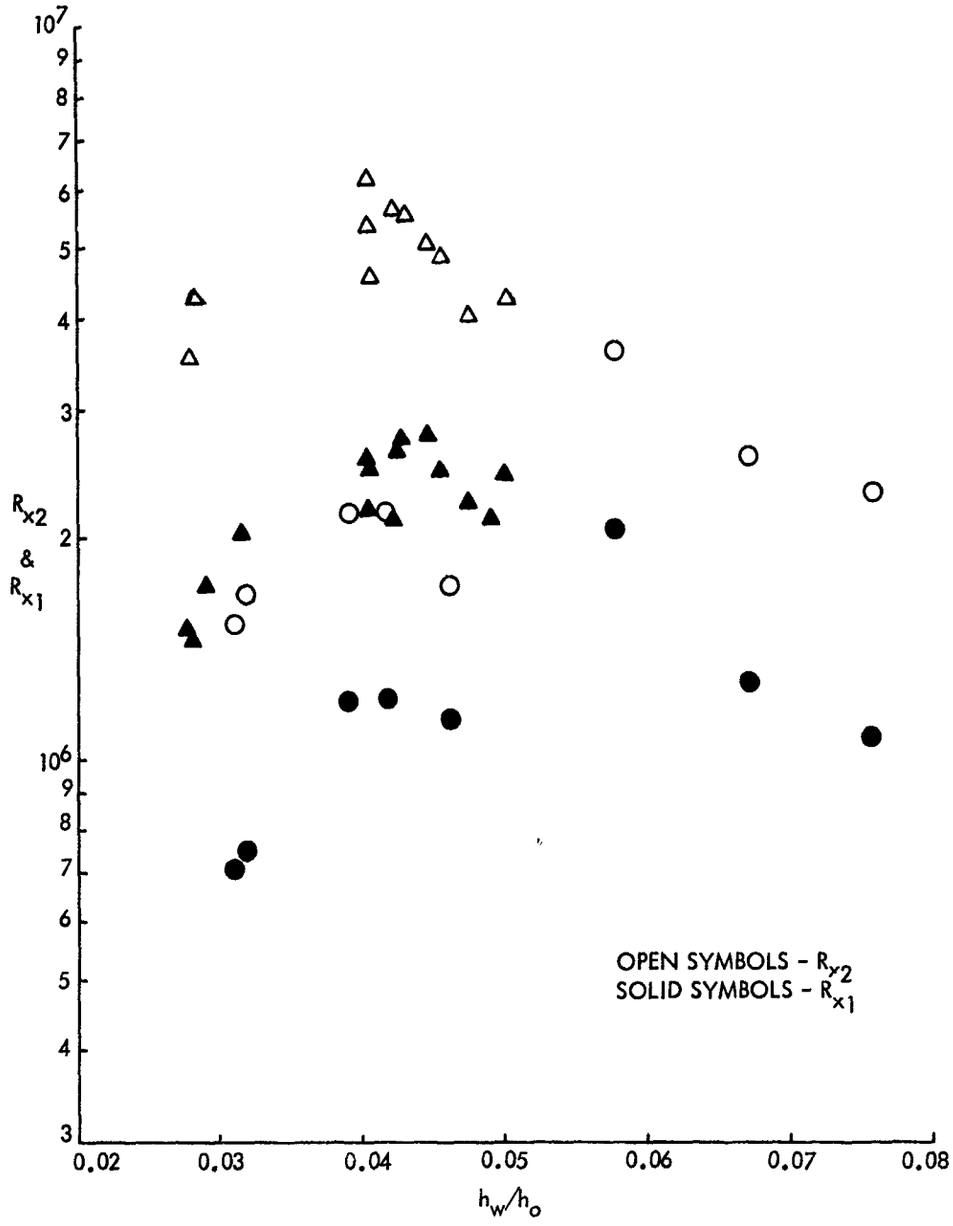

FIG. 5.1 WAKE TRANSITION REYNOLDS NUMBERS AS A FUNCTION OF THE WALL TO STAGNATION ENTHALPY RATIO

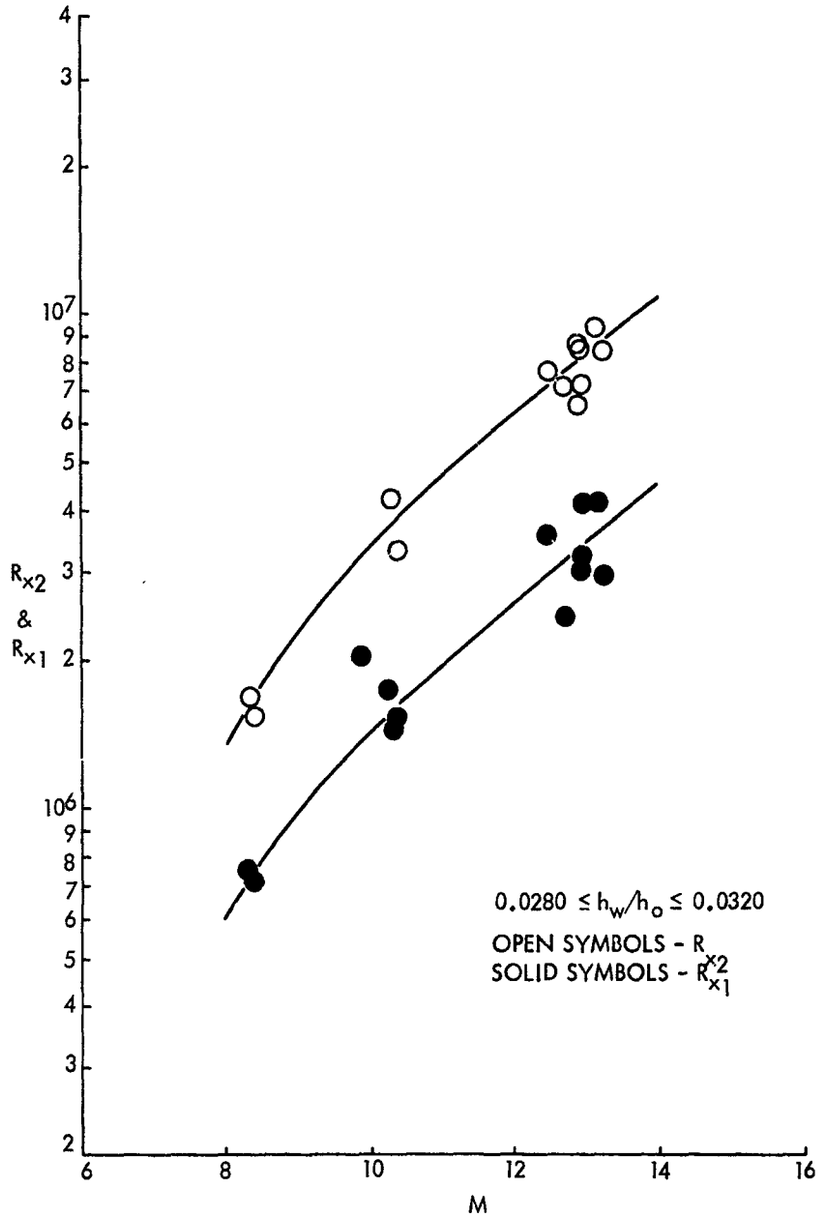

FIG. 5.2 THE EFFECT OF MACH NUMBER ON THE WAKE TRANSITION REYNOLDS NUMBERS

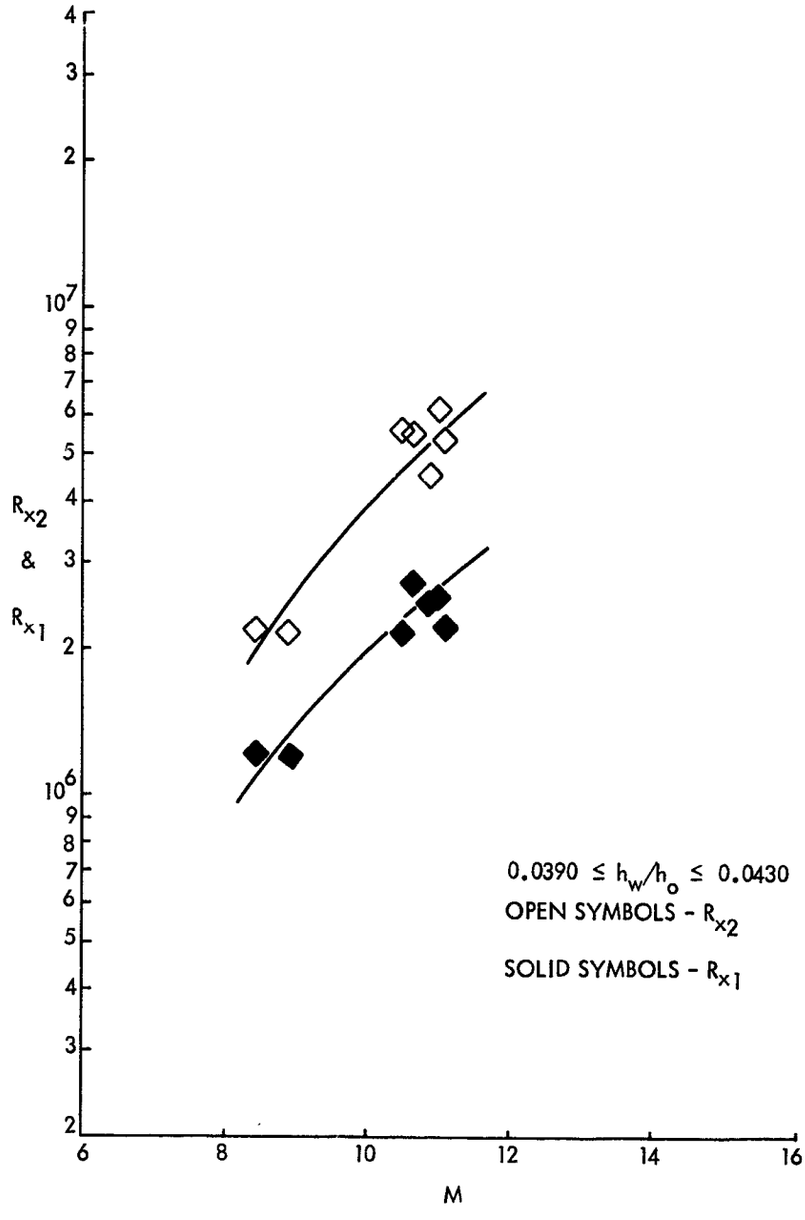

FIG. 5.3 THE EFFECT OF MACH NUMBER ON THE WAKE TRANSITION REYNOLDS NUMBERS

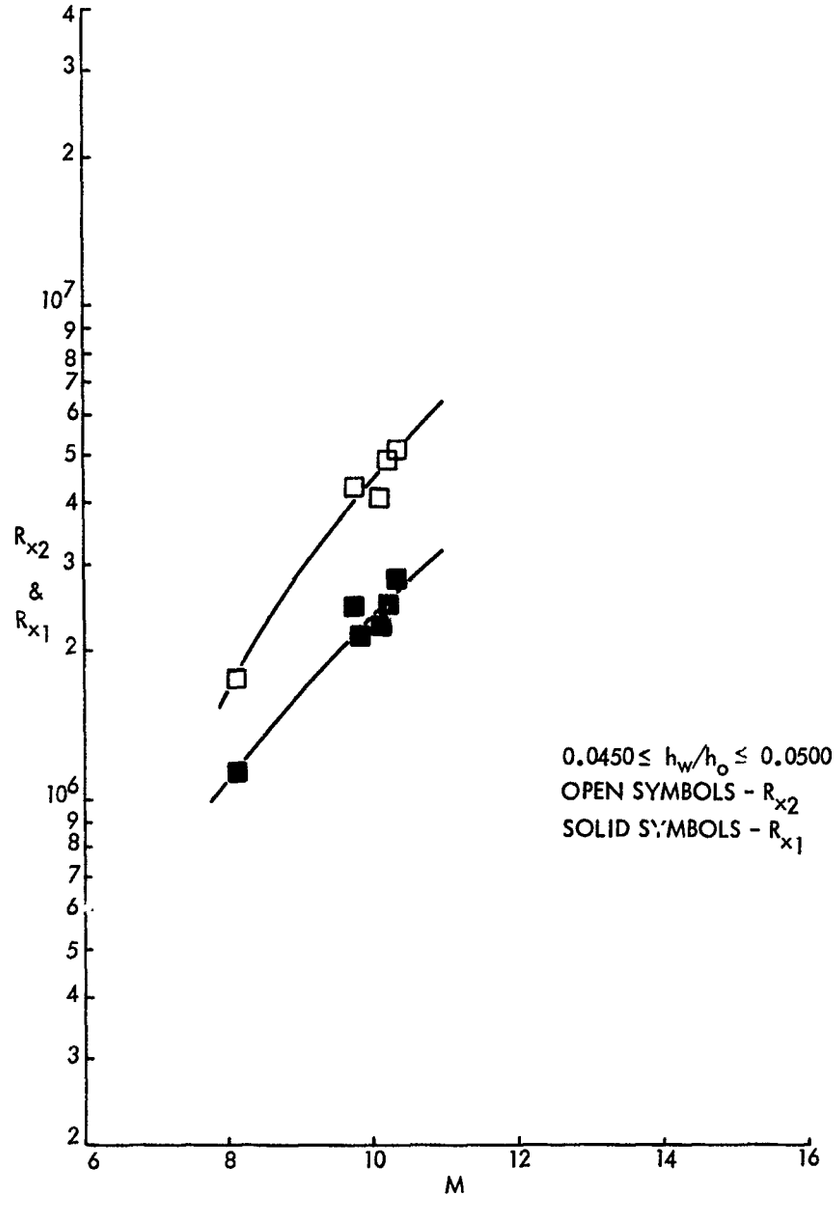

FIG. 5.4 THE EFFECT OF MACH NUMBER ON THE WAKE TRANSITION REYNOLDS NUMBERS

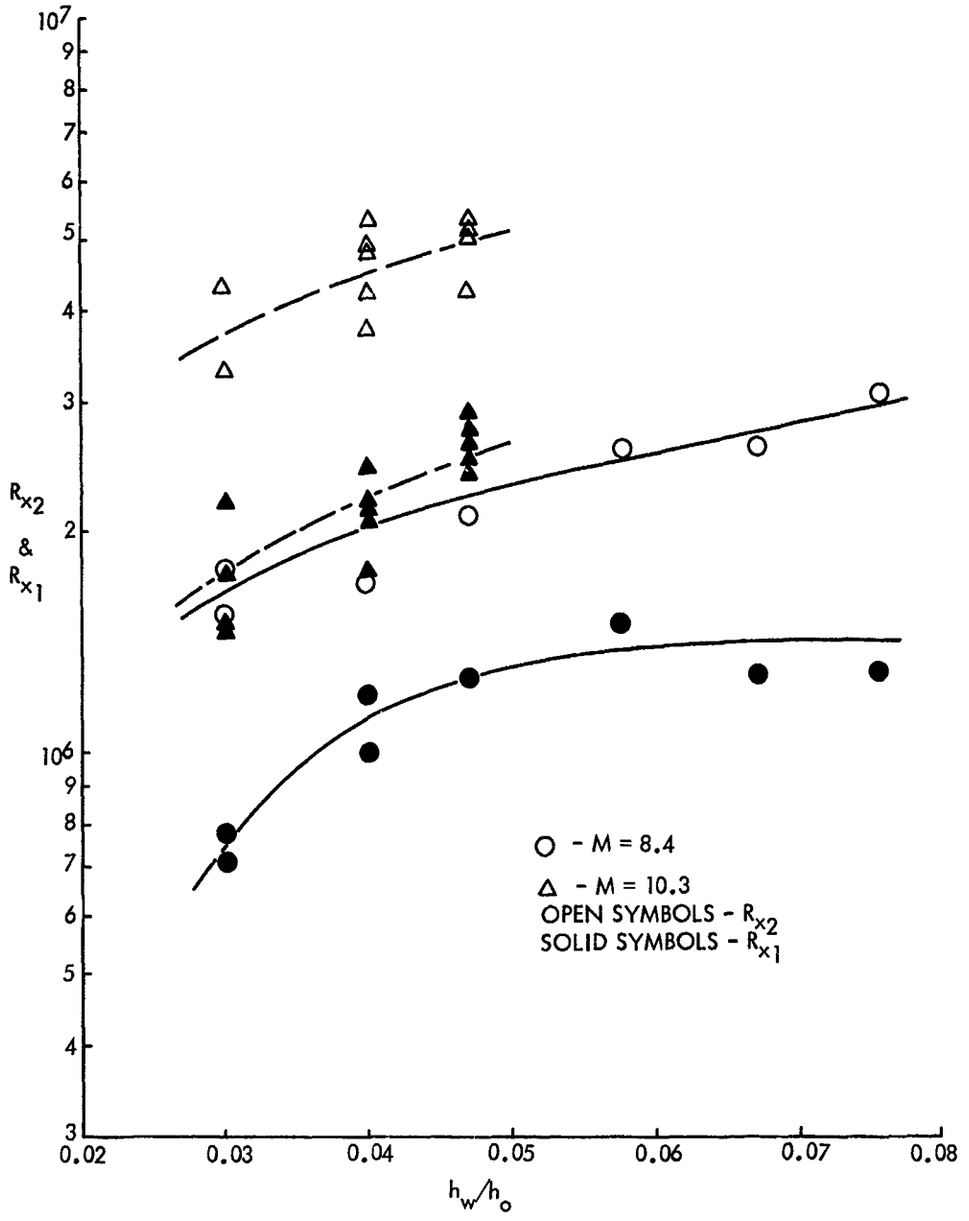

FIG. 5.5 THE EFFECT OF THE WALL TO STAGNATION ENTHALPY RATIO ON THE WAKE TRANSITION REYNOLDS NUMBERS

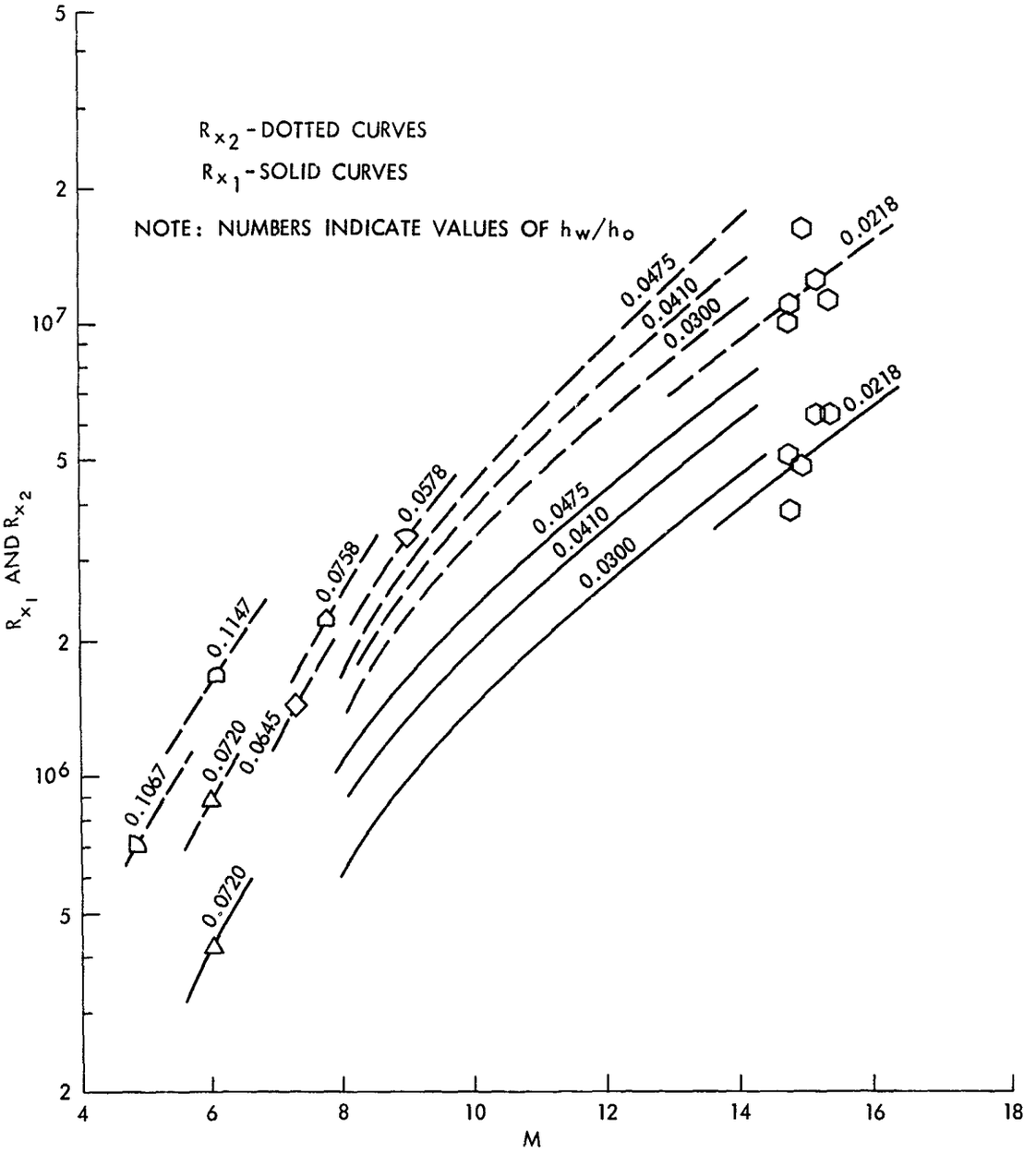

FIG. 5.6 COMPILED RESULTS OF WAKE TRANSITION REYNOLDS NUMBER - MACH NUMBER CORRELATION FOR 9° HALF ANGLE CONES.

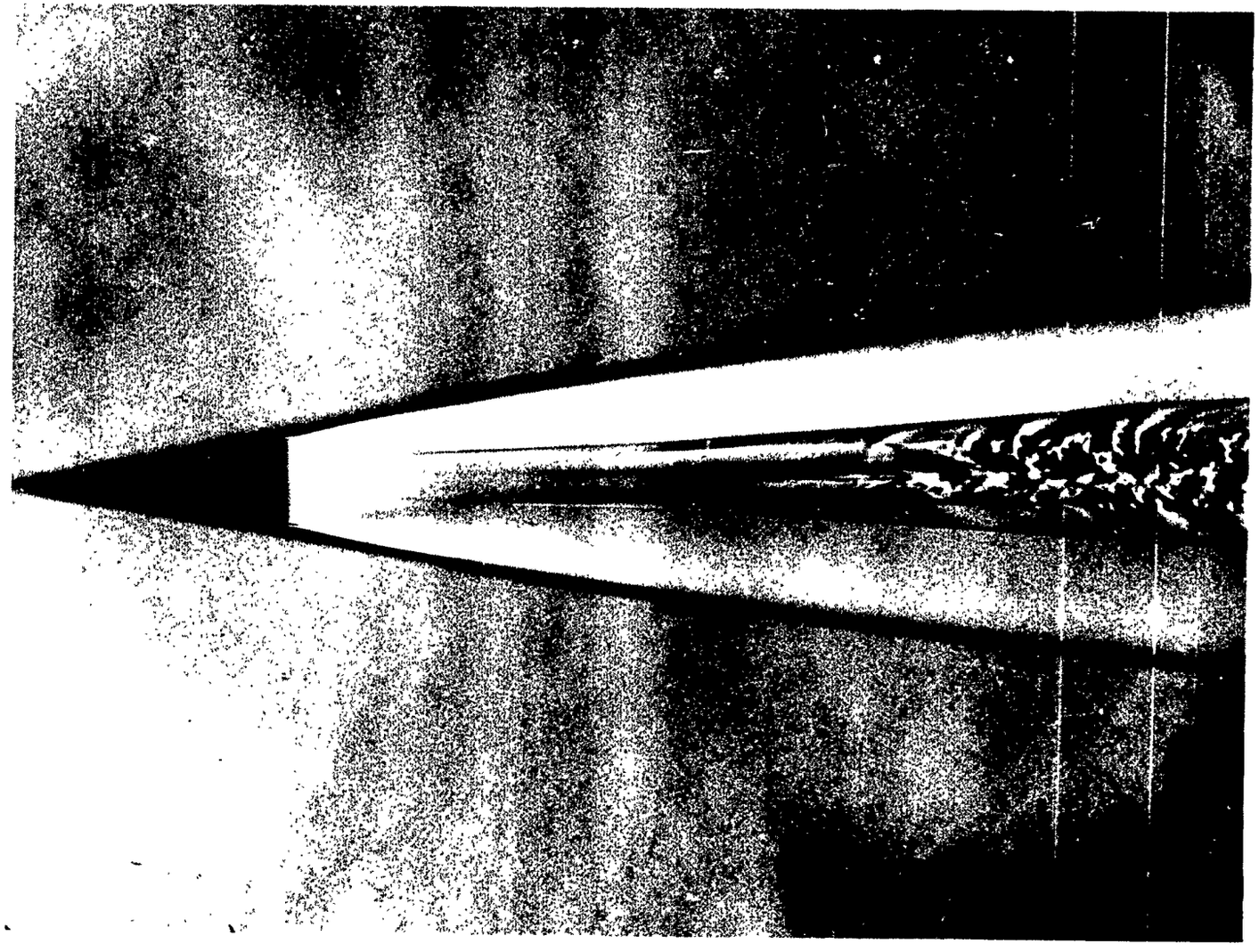

FIG. 5.7 DOUBLE PASS SCHLIEREN PHOTOGRAPH ILLUSTRATING THE BASE FLOW DETAILS

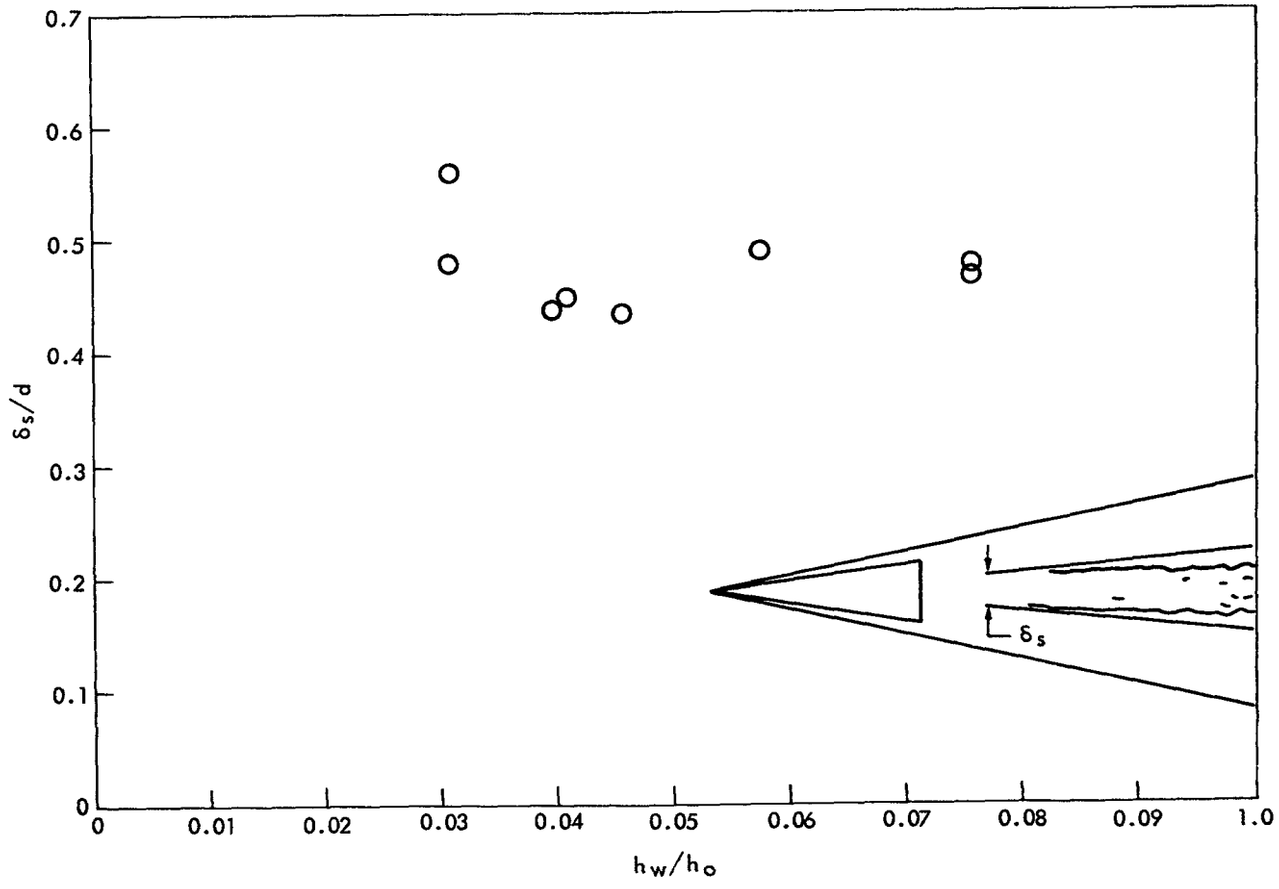

FIG. 5.8 OBSERVED VALUES OF δ_s FOR A RANGE OF WALL TO STAGNATION ENTHALPY RATIOS.
M=8 to 9 R_d=2.1 to 7.1 x 10^5